Molecular Scale Engineering of Functional Conducting Polymer Thin Films

Submitted in partial fulfillment of the requirements for the degree of

Doctor of Philosophy

in

Mechanical Engineering

Phil M Smith

B.S., Applied Mathematics, University of the Virgin Islands

B.S., Mechanical Engineering, Columbia University in the City of New York

M.S., Mechanical Engineering, Stony Brook University

Carnegie Mellon University

Pittsburgh, PA

September 2020

Acknowledgements

I would first like to thank my parents for their continued support throughout my entire educational journey. From encouraging me to enroll in the University of the Virgin Islands to flying all the way to Pittsburgh to help me move into my new apartment when I started grad school. Thanks to my brother Denny and my sister Gizelle for the continuous laughs and always coming to visit when I move to a new city for school. There is never a dull moment when we meet up. Thanks to my niece Lailaa for making my last summer as a grad student one of the most memorable. I look forwards to being there with you as you grow up and navigate your way through this world. Thank you, Amina, for being there for me in my last few years, pushing and motivating me every step of the way.

Next, I would like to thank my academic advisors Professor Reeja-Jayan and Professor Sheng Shen for giving me the opportunity to join their research group. Thank you both for your continued support in both academic and non-academic areas. To the other members of my committee, Professor Michael Bockstaller thank you for providing valuable feedback and comments on the polymer related issues of my work and to Professor Itzhaq Cohen-Karni, thank you for allowing me access to equipment in your lab and giving me the opportunity to collaborate with one of my closest friends, Raghav.

I would like to acknowledge all the member of Professor Jayan’s and Professor Shen’s lab who are great friends, colleagues and collaborators including Nathan, Laisuo, Edgar, Max, Shikhar, Shuyan, Malik, Kyungho, Indorica, Jason, Wei, Jiayui, Bowen, Pengfei, Xiao, Yuxuan, Ramesh, Xiu, Lin, Hyeonggyun, Yusuf and Zhou.

Thank you to all the friends who have been there for me throughout this entire journey. Thank you to the friends I made in Pittsburgh: Satyajit, Dipanjhan, Mayuri, Samy, Sadhana, Kat, Mary, Goran, Steph, Diana, Susana, Anna, Sahil, Neha, Nina, Tom, Francisco, Olga, Steven, Piyumi, Clare, Theo, Wee-Liat, William, Mike, Yun, everyone on my soccer teams Real Apathetico and Yaddie United, Akinlana and the capoeira group. Thank you to the friends I made outside of Pittsburgh: Marvin, Nichelle, Caleb, Sheamal, Buronny, Arianna, Julian, Cherise, Keturah, Wayne.

Finally, I would like to acknowledge the funding sources for this thesis: National science foundation (NSF) - CMMI- 1334630 and the Center for machine learning and health (CMLH) fellowship.

Abstract

In the ever-growing electronics industry, products are constantly being reimagined and tailored around novel materials and processing techniques. Since the discovery of conducting polymers, interest in organic electronics have shifted, as is evident by the rise in market presence of organic light-emitting diodes (OLEDs) which was long the focus of research in academic and industry labs. Lightweight, mechanically flexible, easy to process and low manufacturing costs are a few desirable qualities that conducting polymers have over its inorganic counterparts.

Oxidative chemical vapor deposition (oCVD) polymerization is a new technique that merges CVD thin film processing with the versatility of organic chemistry. This vapor phase polymerization technique offers a facile, solvent-free and low temperature route to simultaneously tune chemistry, morphology and functionality, allowing for creative ways to engineer multiscale (thicknesses from nano to micro) and multifunctional (semiconducting, conducting) polymer films on a variety of substrates including paper, plastic, and biological tissue.

This thesis will study conducting polymers deposited via oCVD from thin film process development, thermal characterization, and various applications in which conducting polymers play a unique role. The deposition parameters for the conducting polymer, poly(3,4-ethylenedioxythiophene) (PEDOT) and the semi conducting polymer, polythiophene (PT) are optimized to create uniform and conformal thin films. Furthermore, the thermal conductivity of oCVD PEDOT is reported for the first time and a relationship to electrical conductivity is determined. This thesis also explores unique applications for these conducting polymers. First, a conducting polymer-based biosensor was utilized for

distinguishing between specific and non-specific binding events. Processing the output data using machine learning resulted in a 75 % accurate prediction of the targeted biomolecule, Biotin. Second, surface modification of a lithium ion battery ($LiMn_2O_4$) electrode with oCVD PEDOT has yielded an 83% increase in rate capacity and a 40 % increase in cycling life. Third, coatings of oCVD PEDOT on 3D graphene structures resulted in the selective and sensitive detection of dopamine among other electroactive species.

Table of Contents

List of Tables

List of Figures

Chapter 1: Introduction

1.1 Motivation

Thin films are classified as materials with thickness ranging from a few nanometers to several micrometers. Compared to their bulk counterpart, thin films possess unique properties due to size constraints, substrate material and deposition process. Typically, the properties of the bulk substrate are unaffected by the deposited thin film, however, the surface properties can be significantly altered. Thin film coatings can be used on glass surfaces allowing for the reflection of heat[1], as a protective coating to minimize unwanted tool wear[2] and as a decorative coating where the color changes based on viewing angle. Furthermore, the surface of glass can become highly conductive while maintaining high optical transparency using transparent conducting oxides (TCOs) and semiconductor thin film materials can transform the surface of different materials into a photovoltaic device.

Functional organic (polymer) thin films are particularly interesting because they play an important role in a wide range of applications from fuel cells and organic light emitting didoes (OLEDs) to antifouling surfaces and biocompatibility of medical implants. Compared to inorganic materials, organic materials have many advantages including, low cost, flexibility, and tunable functionalities. Taking it a step further, polymers can be classified into two categories, electrically conducting and insulating polymers. This dissertation will mainly focus on electrically conducting polymers.

The conjugated structure of alternating single and double bonds present in conducting polymers, give them their intrinsically conducting nature. To every carbon atom there is a

strong sigma bond while every other sigma bond is paired with a weak pi bond. These weak pi bonds cause delocalization of electrons and with the introduction of charged carriers due to doping, the polymer becomes electrically conducting. The first conducting polymer to be discovered was polyacetylene[3] and since then, researchers have focused on developing a library of conjugated polymers. In this area of study, the long-term goal is to create materials which demonstrate properties of metals or inorganic semi-conductors while still maintaining the desirable mechanical properties and facile processability of polymers. A few common examples are polypyrrole (PPy), polyaniline (PANI), polythiophene (PT) and poly(3,4-ethylenedioxythiophene) (PEDOT). PEDOT has become one of the most well-known and widely used conducting polymers[4][5]. In addition to high electrical conductivity, it has long-term stability in air, long-term stability at high temperatures and is easy to process.

There are multiple ways in which PEDOT can be deposited. In the electropolymerization of PEDOT films, the substrate acts as one of the working electrodes which is placed in an electrolyte containing the monomer 3,4-ethylenedioxythiophene (EDOT). The practical application of this technique is limited since the surface of the substrate must already be electrically conducting. To make PEDOT soluble in polar solvents such as water, poly(styrenesulfonate) (PSS) is added. This makes the conducting polymer more accessible since common processing techniques such as spin coating[6] and screen printing[7] can be used. In both cases, controlling film thickness is difficult, especially on the nanoscale. If the monomer and oxidant are applied separately, more flexibility in terms of tunable parameters is achieved. Vapor phase polymerization (VPP) and oxidative chemical vapor deposition (oCVD) are techniques which can be used. VPP is a two-step

process which entail first applying oxidant to the substrate, followed by exposure of the oxidant coated substrate to monomer vapors inside of a sealed container[8]. oCVD, on the other hand, is a one-step all vapor technique which eliminates the need for solvents. Both the monomer and oxidant are in the vapor phase and polymerization and thin film formation occur simultaneously on the substrate surface. This leads to new and unique applications which cannot be realized with the previously mentioned techniques[9]. This will be discussed further in chapter 2.

One important consideration for using these polymer thin films is choosing the right deposition process. Nearly every property of thin films such as electrical, optical and microstructure, can be altered by the deposition process. As a result, the deposition process must be chosen to fit the specific application. oCVD is a relatively new technique and as such there are many areas to study and applications that have yet to be explored. The electrical properties of oCVD films have been extensively studied[10] however thermal properties in many of these oCVD polymers are not well understood. Knowing the thermal behavior of a material is also an essential factor for material selection. Polymers are typically known for having low thermal transport properties which can lead to an increase in temperature and polymer degradation. This can lead to a reduction in the lifetime of organic electronics and a decrease in electrical conductivity[11]. As a result, understanding thermal transport is important for the overall performance and lifetime of organic electronics.

1.2 Scope of Thesis

The objective of this thesis is to study the thermal conductivity of oCVD polymer films and demonstrate the use of conducting polymers in various applications and device structure. The conducting polymers studied here are poly(3,4-ethylenedioxythiophene) (PEDOT) and polythiophene (PT). The thermal conductivity of oCVD PEDOT films are reported for the first time and the process development for oCVD PT thin films are described. Applications that highlight the unique characteristics of the oCVD process such as thickness control and conformality are demonstrated.

Chapter 2 reports on the main methods used in this thesis. The oCVD process is reviewed and the experimental process used in this thesis is reported. Exact process parameters are reported in more detail. The differential 3ω method is introduced, and the sample preparation developed to measure the thermal conductivity of polymer thin films is reported.

Chapter 3 reports the thermal conductivity of oCVD PEDOT films for the first time. A relationship between the thermal conductivity and electrical conductivity as a function of substrate temperature during deposited is also discussed.

Chapter 4 reports on process development for unsubstituted Polythiophene thin film deposition using iron (III) chloride ($FeCl_3$). Raman spectroscopy and scanning electron microscopy are used to characterize and image the deposited films.

In chapter 5, PEDOT is utilized in a conducting polymer-based chemiresistive biosensor for distinguishing between specific and non-specific binding events. The sensor's ability

to detect a targeted protein in a dual protein analyte solution using machine learning classifiers is also demonstrated.

Chapter 6 provides an overview on collaborative work done with oCVD PEDOT on high surface area devices. oCVD PEDOT was well suited for these applications due to its conformal nature and control over film thickness. In this chapter, oCVD PEDOT is applied in lithium ion batteries where conformality of the film is important. It is also applied as a coating on a 3D graphene structure, creating a hybrid material that can be applied to dopamine sensing.

Chapter 7 discusses future work and upgrades that can be made to the oCVD reactor and the deposition process.

Chapter 2: Methods

2.1 Oxidative Chemical Vapor Deposition (oCVD)

Molecular scale engineering tools like chemical vapor deposition (CVD) are the workhorses of the microfabrication industry. With these primarily inorganic thin film coating technologies, one can achieve multifunctional properties on the surface of a material which are different from those of the underlying substrate. CVD polymerization is a new technique that merges CVD thin film processing with the versatility of organic chemistry. This vapor phase polymerization technique offers a facile, solvent-free and low temperature route to simultaneously tune chemistry, morphology and functionality, allowing for creative ways to engineer multiscale (thicknesses from nano to micro) and multifunctional (insulating, semiconducting, conducting) polymer films on a variety of substrates including paper, plastic, and biological tissue[10]. Although there are many similarities between CVD of inorganic materials and CVD of polymers, there are also differences as it pertains to deposition rate, conformality and film properties.

When optimizing the growth parameters for a polymer thin film deposition, the stage temperature is crucial in obtaining high quality films. Higher stage temperatures lead to lower deposition rates due to a reduction in adsorption and promotes the growth of long chains thus increasing conjugation. Lower stage temperature promotes monomer adsorption leading to an increase in deposition rate [15]. The volatility of the reactants must be taken into consideration when optimizing this parameter. In inorganic CVD, this relation is the opposite up to a certain temperature. Increasing substate temperature would result in an increase in deposition rate due to an acceleration in the kinetics of the thermally activated surface reaction step. However, increasing the temperature

sufficiently high, reduces the effect of the surface reaction step slowing down the deposition rate. In this case, mass transport of the reactants has a greater effect on the deposition rate[12]. For oCVD, the oxidant delivery rate strongly affects the deposition rate. An increase in deposition pressure results in an increase in the monomer surface concentration. However, higher oxidant heating temperatures are required to obtain comparable film growth rates at higher pressures[13]. This suggests that the oxidant delivery rate and not the monomer delivery rate has a greater effect on the deposition rate.

The monomer adsorption is an important step in CVD polymerization and can be determined from the saturation ratio (S) given by P_m/P_{sat}, the ratio of the partial pressure of the monomer to its saturation pressure. This quantity can also be used to determine the degree of conformality and growth rate. The partial pressure of the monomer can be directly determined from the flow rates of the reactants and the deposition pressure, while the saturation pressure can be estimated using the Claussius-Claperyon relationship. Knowledge and control of the saturation ratio is crucial in film growth. If the saturation ratio is 1, then condensation will occur in the reactor which will cause run to run variability. On the other hand, if the saturation ratio is much less than 1 then film growth rate will be extremely slow[14]. 3

Creating a film with uniform thickness over samples with micro/nano scale geometries is a feat achievable only with vapor deposition techniques. In CVD polymerization, this conformal coverage is highly dependent on the sticking coefficient which is the probability a reactant adsorbs on a surface each time it strikes it. Low sticking coefficients allow for deposition inside high aspect ratio features. The saturation ratio also affects the sticking

coefficient. The sticking coefficient increases as the surface adsorption increases. By decreasing the saturation ratio, the sticking probability also decreases which results in better step coverage[15]. In oCVD, to account for the low volatility of certain oxidants, crucibles placed inside the CVD reactor are used for delivery. This makes determining the saturation ratio difficult since the flow rate of the oxidant is unknown. For this reason, optimizing the deposition for increased conformality is more challenging. More volatile oxidants like Bromine gas can be used to obtain better conformality because the sticking coefficient is lower than that of the solid oxidants which are typically used[16].

As depicted in figure 2.1 (a), the all-dry oCVD thin film polymerization process involves subliming and reacting a solid-state oxidant like iron (III) chloride ($FeCl_3$) with heated vapors of the monomer (EDOT, thiophene). Polymerization and thin film coating occur simultaneously onto the surface of a temperature-controlled stage placed inside the custom-designed oCVD reactor. Figure 2.1 (b) shows a picture of the reactor. The tall design of the reactor accounts for the presence of the evaporators which are housed inside the reactor chamber. The system is equipped with 3 monomer feed lines which would allow for the simultaneous introduction of multiple chemicals in the vapor phase. One of these lines has a heated mass flow controller (MFC) while the other two have needle valves. The system is equipped with two thermal evaporators to allow for co-evaporation of multiple materials. The rotating stage can attain temperatures from 10 – 170℃.

Polymerization in the oCVD is a spontaneous reaction and does not require the input of energy from high stage temperatures, a heated filament or plasma for the polymerization to progress. The polymerization of EDOT proceeds via step-growth polymerization shown

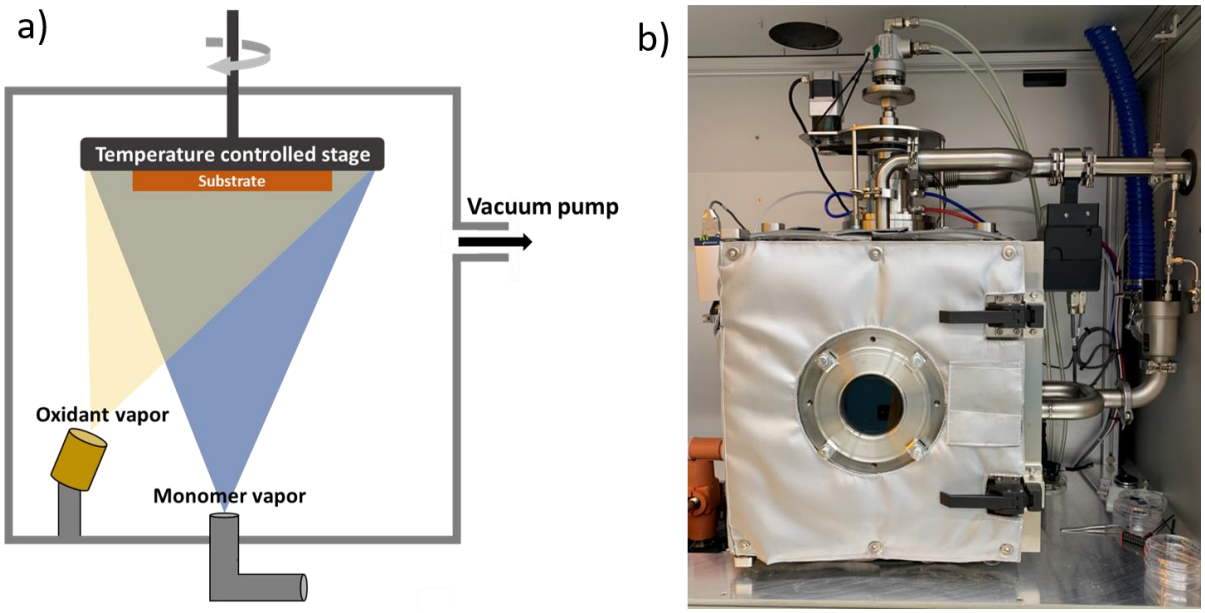

Figure 2.1 (a) Schematic of oCVD reactor (b) Picture of the oCVD reactor.

in figure 2.2[17]**.** The oxidant initiates the reaction by removing an electron from EDOT forming a radical cation. These radicals are highly reactive and form new bonds with another radical cation providing carbon-carbon coupling. The anion of the oxidant then takes two hydrogen ions from the newly coupled carbon, stabilizing it. This process is then repeated to form the polymer. Finally, the undoped polymer is doped with the anion of the oxidant (X = Cl-, PTS-, Br-).

In some electronic applications, patterning thin films into specific geometries and dimensions are necessary. Creating these patterns of conducting polymers by simply using a shadow mask does not place any restrictions on the type of substrate that can be used. Even a material like paper can be used to make a photovoltaic device[18]. 3D micro/nano structures such as inverted pyramids or carbon nanotubes are often used as enhancement techniques[19,20]. The ability to follow the geometry of these structures is

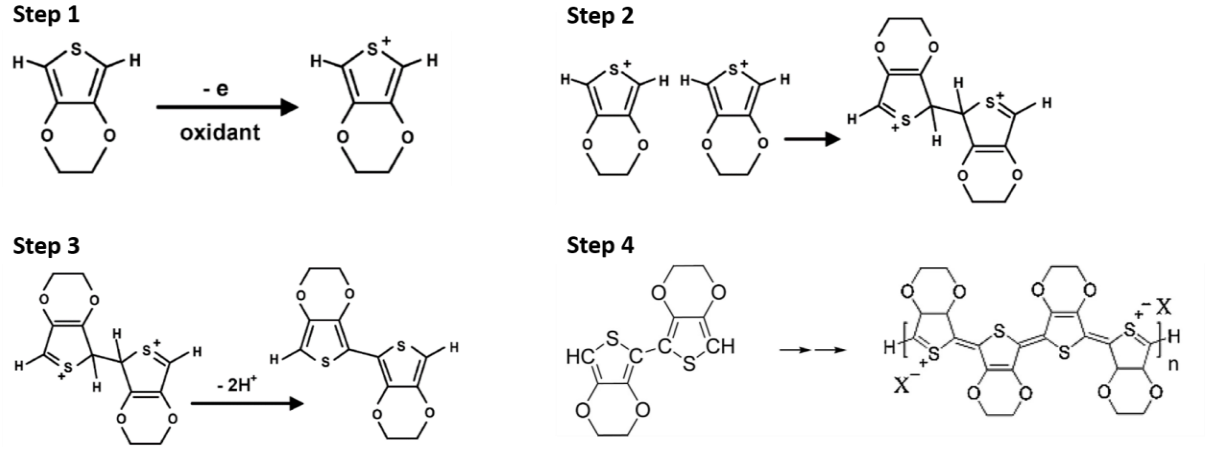

Figure 2.2 EDOT polymerization mechanism.

one of the major highlights of the oCVD technique as opposed to the solution-based technique where voids in the film could form on such length scales. As mentioned earlier in chapter 1, the way in which these thin films are created can have a significant impact on its properties and oCVD PEDOT is no exception. Increasing the stage temperature during the deposition leads to an increase in the doping level and provides the ability to tune the work function[21]. The addition of water vapor during the oCVD process has been shown to promote the packing of the PEDOT chains leading to a change in morphology and doping level[22]. Similarly, structural changes are seen when the oxidant is changed from a solid like iron chloride to a gas like Bromine[16]. These highly volatile oxidants also have the added benefit of being more controllable. Post deposition rinsing in an acid such as hydrobromic acid (HBr) has also been shown to increase conductivity[23].

2.2 The 3ω Method

2.2.1 Bulk Samples

The 3ω method used to measure the cross-plane thermal conductivity of bulk samples is classified as a transient technique where a metal line acts simultaneously as a source heater and thermometer[24][25]. For this reason, this technique is limited to samples that are electrically insulating to prevent inaccuracies caused by current leakage. A schematic of the metal line on a bulk sample is shown in figure 2.3. A sinusoidal current at frequency ω is passed through the metal line given by

$$I = I_0 \cos(\omega t) \qquad 2.1$$

where I_0 is the amplitude of the current. This results in joule heating which causes the temperature of the line to oscillate at a frequency of 2ω. This temperature oscillation (ΔT) is given by[26],

$$\Delta T = \Delta T_{DC} + \Delta T_{AC} cos(2\omega t + \theta) \qquad 2.2$$

where ΔT_{DC} and ΔT_{AC} are the DC and peak AC temperature rise respectively and θ is the phase angle. Furthermore, the resistance of a metal is proportional to the temperature, given by

$$R = R_0(1 + \beta \Delta T), \qquad \beta = \frac{1}{R_0}\frac{dR}{dT} \qquad 2.3$$

where R_0 is the resistance of the metal line at temperature T_0, β is the temperature coefficient of resistance (TCR) and $\frac{dR}{dT}$ is the change in resistance of the line with respect to temperature. It follows that the resistance of the metal line also has a component oscillating at 2ω. The temperature oscillation can be experimentally determined from the

voltage (V=IR) across the line. The expression for the voltage can then be determined by combining equations 2.1, 2.2 and 2.3**.** This voltage expression contains a component oscillating at a frequency of 3ω. This voltage component is much smaller than the 1ω component and the amplitude ($V_{3\omega}$) is given by

$$V_{3\omega} = \frac{1}{2} I_0 R_0 \beta \Delta T_{AC}. \qquad 2.4$$

The exact solution for ΔT_{AC} as a function r (distance from line heater) is given by[27]

$$\Delta T_{AC}(r) = \frac{P}{\pi k l} K_0(qr), \qquad q = \sqrt{i2\omega/\alpha} \qquad 2.5$$

where P is the power dissipated, *k* is the thermal conductivity, l is the length of the line, K_0 is the zero-order modified Bessel function and α is the thermal diffusivity. The thermal penetration depth is defined as the magnitude of *1/q*. For $|qr| \ll 1$, equation 2.5 can be approximated to[28]

$$\Delta T_{AC} = \frac{P}{\pi k l}\left[\frac{1}{2} ln\left(\frac{\alpha}{r^2}\right) + ln2 - 0.5772 - \frac{1}{2} ln\omega - \frac{i\pi}{4}\right]. \qquad 2.6$$

Using the frequency dependent term, the slope of ΔT_{AC} vs ln(ω) can be used to determine the thermal conductivity.

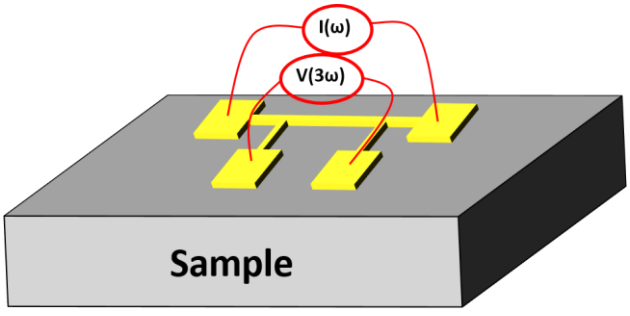

Figure 2.3: Schematic of a bulk sample with 3ω metal line

2.2.2 Thin Films

The submicron thickness of thin films poses a challenge for the conventional 3ω method. One of the conditions for this technique is that the thermal penetration depth must be smaller than the thickness of the sample being measured. This restricts the film thickness to > 30 µm[24]. An extension of the conventional 3ω method was developed to allow for the measurement of thin films[29]. Figure 2.4 (a) shows a schematic of the device structure for measurement. During my PhD studies, I built the measurement setup for performing 3ω measurements on thin films and developed a sample preparation technique for measuring conducting polymer thin films. In this work, the conducting polymer is deposited on a silicon wafer with a thermally grown silicon dioxide oxide layer. A 100 nm thick blocking layer of the electrically insulating polymer, poly (divinylbenzene) (PDVB), was deposited on the PEDOT layer to prevent current leakage. The experimental setup is like the bulk sample setup except for the presence of a thin film. In this case, however, the width of the line heater must be large compared to the film thickness for 1D heat flow. By depositing the film on a substrate with a much higher thermal conductivity,

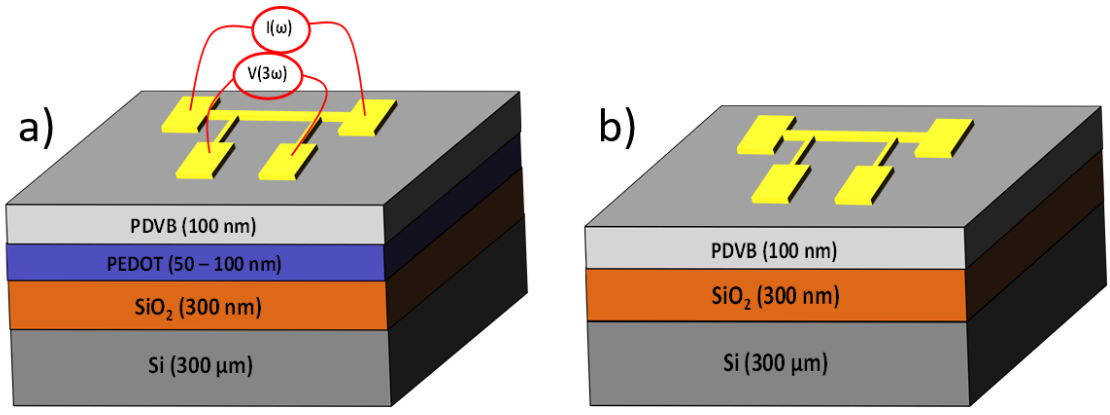

Figure 2.4 Schematic of (a) sample containing conducting polymer film (b) reference sample without conducting polymer

the film adds a frequency independent component to the temperature oscillation. As such, the temperature oscillation of the entire sample (ΔT_{Total}) is given by

$$\Delta T_{Total}(\omega) = \Delta T_{Sub}(\omega) + \sum_{i=1}^{n} \Delta T_i \qquad 2.7$$

where ω is the angular frequency, ΔT_{Sub} is the component of ΔT_{Total} caused by the substrate, ΔT_i is the component of ΔT_{Total} caused by the *i*-th film, and n is the total number of films on the substrate. To determine the component of the temperature oscillation caused by the film of interest, the contributions from other films need to be known. To simplify this analysis, a differential 3ω method is used. The main idea behind this is to create a set of identical samples except for the film of interest. An example of this is shown in figure 2.4**.** The reference sample in figure 2.4 (b) is identical to the sample in figure 2.4 (a) except for the PEDOT film. The difference between the temperature oscillation of these two samples will be solely due to the presence of the PEDOT film. As such, the component of the temperature oscillation caused by the film (ΔT_f) is simply

$$\Delta T_f = \Delta T_{Total}(\omega) - \Delta T_{ref}(\omega) \qquad 2.8$$

where ΔT_{ref} is the temperature oscillation from the reference sample. This can be seen in figure 2.5**.** Once ΔT_f is known, the thermal conductivity of the film (k_f) is calculated using

$$k_f = \frac{P\, t_f}{L\, W\, \Delta T_f} \qquad 2.9$$

where t_f is the thickness of the film and P, L and W are the power, length, and width of the line heater, respectively.

2.2.3 Sample Preparation

The conducting polymer films measured using the 3ω method were all deposited using the oCVD technique described in section 2.1. The first step in the sample preparation is

to deposit an insulating layer on the polymer surface to electrically insulate the conducting polymer from the metal line. A 100 nm thick film of the electrically insulating polymer, poly (divinylbenzene) (PDVB), deposited using initiated chemical vapor deposition (iCVD) was used.

The metal line was made up of gold (100 nm) and a thin adhesion layer of chromium (10 nm) deposited using an Ultek e-beam evaporator. To obtain the designed geometry of the metal lines, photolithography was initially used. However, this method was quickly abandoned. Due to the many steps involved in the photolithography process, the polymer film showed signs of cracking and delamination after all the steps were completed. Furthermore, wire bonding to these contact pads were unsuccessful and the pads were damaged in the process (figure 2.6 (a))**.** A shadow mask became the next viable option. The parameters of a LPKF ProtoLaser U3 were tuned to cut a 75 µm thick stainless-steel

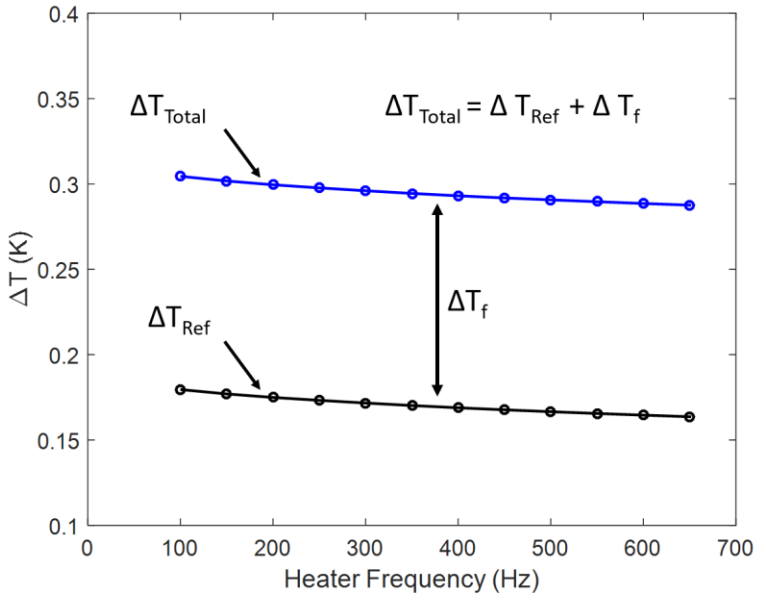

Figure 2.5 Measured temperature oscillation vs frequency for the sample containing the PEDOT layer and reference sample. The component of the temperature oscillation caused by the PEDOT layer is the difference between the two signals.

sheet. Shadow masks mounted onto samples before metal deposition are shown in figure 2.6 (b). The resulting metal lines were 40 – 70 µm wide and ~2000 µm long. Once the metal is deposited and the shadow mask removed, the samples were manually diced and placed on a 24-pin dual in-line ceramic package (DIP) (figure 2.6 (c)). A Westbond 7476D wedge wire bonder was used to create electrical connections between the metal line and the DIP. However, due to the delicate and soft nature of the polymer films, directly bonding to the metal line contact pads resulted in damage and bond detachment. To facilitate the wire bonding process, the technique employed by Kaul et al.[30] was modified and used. A small amount of conductive epoxy was first applied to each contact pad. After curing, wire bonding was then done directly from the solid epoxy to the DIP (figure 2.6 (d)).

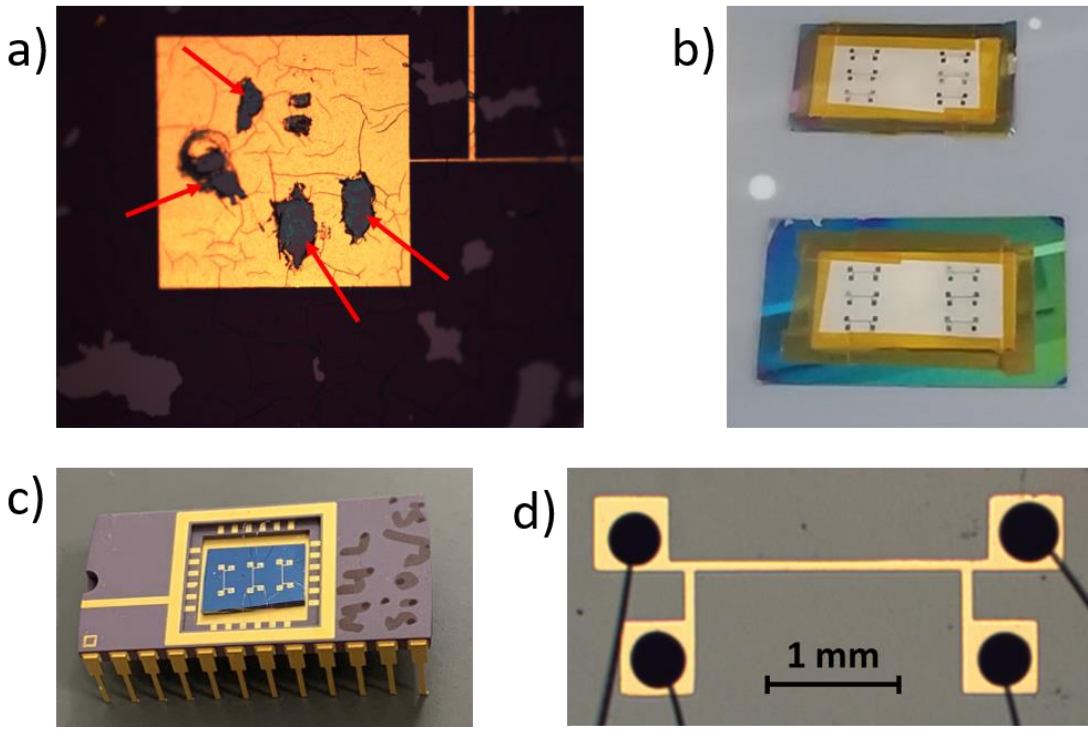

Figure 2.6 (a) Contact pad (400 µm x 400 µm) of metal line created using photolithography. The red arrows show damaged area after wire bonding. (b) Stainless steel shadow mask mounted onto sample. (c) Sample mounted onto 24 pin Dual In-Line Ceramic Package (DIP). (d) Metal line heater with conductive epoxy and bonded wires.

2.2.4 Experimental Setup

All measurements were performed in a Jantis ST-500 cryostat cooled with liquid nitrogen. The pressure is maintained to about 10^{-7} Torr. This minimizes conduction and convection heat transfer from the top of the metal line to the environment. A schematic of the experimental setup is shown in figure 2.7. A Keithley 6221 DC and AC current source meter was used to supply the current to the metal line, two differential amplifiers were used to measure the voltage difference across the metal line and the potentiometer and a 50 Ω resistor was used to provide a reference input for the lock-in amplifier (Stanford Research Systems SR800). The potentiometer was used to match the 1ω signal from the metal line. This allowed the 3ω signal to be isolated by the lock-in amplifier. Initially, a

solderless breadboard was used to create the circuit however these are only good for prototyping, solderable breadboards provide better connection between electrical components. As a result, an acrylic box was constructed to house the electrical components which include all BNC inputs and outputs needed for the input current, metal line, the lock-in amplifier and ground. A MATLAB GUI was created to control the measurement equipment and data collection and processing. The uncertainty in the measurements was calculated using the Kline Mcklintock method[31].

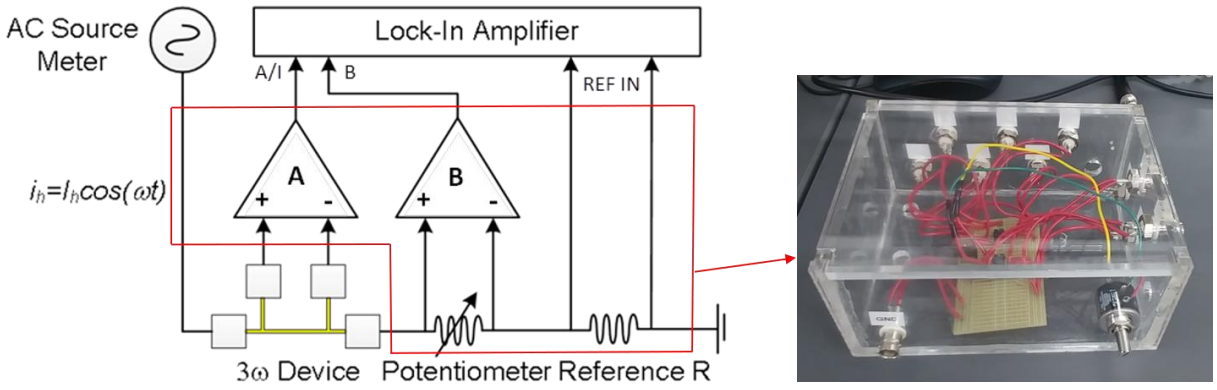

Figure 2.7 Schematic of experimental setup for 3ω method. An acrylic box was constructed to house all the electrical components and contained BNC connections for the input sinusoidal current, metal line, lock-in amplifier, and ground.

Chapter 3: Thermal Conductivity of PEDOT Thin Films Prepared by oCVD

3.1 Abstract

Oxidative chemical vapor deposition (oCVD) is a versatile technique that can simultaneously tailor properties (e.g., electrical, thermal conductivity) and morphology of polymer films at the nanoscale. In this work, we report the thermal conductivity of nanoscale oCVD grown poly(3,4-ethylenedioxythiophene) (PEDOT) films for the first time. Measurements as low as 0.16 W/m·K are obtained at room temperature for PEDOT films with thicknesses ranging from 50 - 100 nm. These values are lower than those for solution processed PEDOT films doped with the solubilizing agent PSS (polystyrene sulfonate). The thermal conductivity of oCVD grown PEDOT films shows no clear dependence on electrical conductivity, which ranges from 1 S/cm to 30 S/cm. It is suspected that at these electrical conductivities, the electronic contribution to the thermal conductivity is extremely small and that phonon transport is dominant. Our findings suggest that CVD polymerization is a promising route towards engineering polymer films that combine low thermal conductivity with relatively high electrical conductivity values.

Publication[32]**:** Smith P.M. et al, RSC Adv., 2018, 8, 19348

3.2 Introduction

Oxidative chemical vapor deposition (oCVD) is the vapor phase equivalent of solution-based oxidative (step growth) polymerization. oCVD enables the polymerization of thin films of electrically conducting polymers such as poly(3,4-ethylenedioxythiophene) (PEDOT)[10][33]. Due to its high electrical conductivity, optical transparency, mechanical flexibility, and chemical and physical stability, PEDOT is one of the most widely studied

conducting polymers[4]. Commercially available PEDOT solutions are a mixture of PEDOT with the surfactant poly(styrenesulfonate) (PSS). This surfactant enables the dispersion of PEDOT in polar solvents, making processing techniques such as spin coating[6] and screen printing[7] a viable option for depositing PEDOT thin films. However, the highly polar PSS is strongly acidic and can cause failure in devices such as polymer solar cells[34]. Although solution processing techniques may be widespread, realizing nanoscale film thicknesses will often lead to non-uniformity due to de-wetting and surface tension effects that accompany solution processes.

De-wetting and surface tension also make textured surfaces[35] difficult to coat with the aqueous PEDOT:PSS while preserving the morphology of the structure underneath. On the other hand, CVD polymer films are uniform and pinhole free, exempt from de-wetting and surface tension effects. For this reason, extremely thin films are also attainable. In oCVD, reactants arrive at textured surfaces from all sides in the vapor phase, resulting in completely conformal PEDOT films that follow the contours of complex geometries[36][19].

The vapor phase CVD process is further compatible with substrates which would dissolve or degrade in the presence of solvents. This enables the creation of devices on fragile materials such as paper[18] which would lose its structural integrity if exposed to any type of solvent. Copolymerization is also possible, providing access to functional groups which are not inherent to the specific polymer of interest[37]. The low cost, mechanical flexibility and varied functionality offered by CVD polymerization is thus unmatched by existing solution processing methods.

Herein, we use the differential 3ω method to measure the thermal conductivity of oCVD grown PEDOT films for the first time. In the oCVD process, by simply changing the substrate temperature, the conjugation length of the conducting polymer can be modified, thereby altering the electrical conductivity[38]. We studied the thermal conductivity of films grown at different substrate temperatures to determine whether a correlation exists between thermal and electrical conductivity. The well-known transmission line method (TLM) was used to measure the electrical conductivity.

3.3 Methods

3.3.1 oCVD PEDOT Deposition

The deposition conditions used are summarized in table 3.1. The oCVD procedure has been previously report by Im et al.[38]. Briefly, the monomer (EDOT) was placed in a stainless-steel jar and heated to 130 ˚C. The samples were placed on a heated rotating stage maintained at temperatures outlined in Table 3.1. The EDOT and Argon were introduced into the chamber at 2 sccm and 1 sccm respectively and the oxidant was sublimed at 225 ˚C. The depositions were conducted at a pressure of 100 mT for 45 mins. The samples were then rinsed in methanol for 5 mins before further measurements were conducted.

The thickness of the oCVD PEDOT films were measured using a KLA Tencor P-15 profilometer. The film was scratched in multiple locations to expose the underlying substrate such that the film thickness can be measured. For this, a soft tip tweezer was used to avoid placing scratches in the substrate itself. The thickness was measured at multiple locations across the sample and then averaged. In a separate set of experiments, the uniformity of the oCVD PEDOT films were measured using ellipsometry, results are

shown in figure 3.1 and table 3.2. The FTIR spectrum of the oCVD film is shown in figure 3.2. The C=C asymmetric stretching mode is seen at 1516 cm-1, the C-C inter-ring stretching mode is seen at 1317 cm-1, the peaks appearing from 1188 cm-1 to 1053 cm-1 corresponds to the C-O-C bending vibration in ethylenedioxy group and the peaks appearing from 977 cm-1 to 837 cm-1 corresponds to the C-S-C stretching vibration in the thiophene ring.

Table 3.1 Summary of oCVD PEDOT deposition parameters

Substrate temperature (˚C)	70	100	130
Monomer flow rate (sccm)	2	2	2
Argon (sccm)	1	1	1
Chamber pressure (mT)	100	100	100
Evaporator temperature (˚C)	225	225	225
Deposition time (mins)	45	45	45

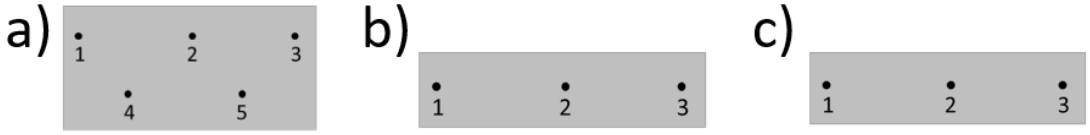

Figure 3.1 PEDOT thin films on Si wafer for different coating time. a) 5 mins, b) 10 mins, c) 20 mins. The points with number beside them are positions during ellipsometry measurement.

Table 3.2 PEDOT Film thickness measured by ellipsometry at different locations for three different samples, as shown in figure 3.1

Point		1	2	3	4	5
Thickness (nm)	Sample 1	13.9	15.9	13.8	15.1	15.6
	Sample 2	22.9	22.3	22	/	/
	Sample 3	49.3	48.4	48.6	/	/

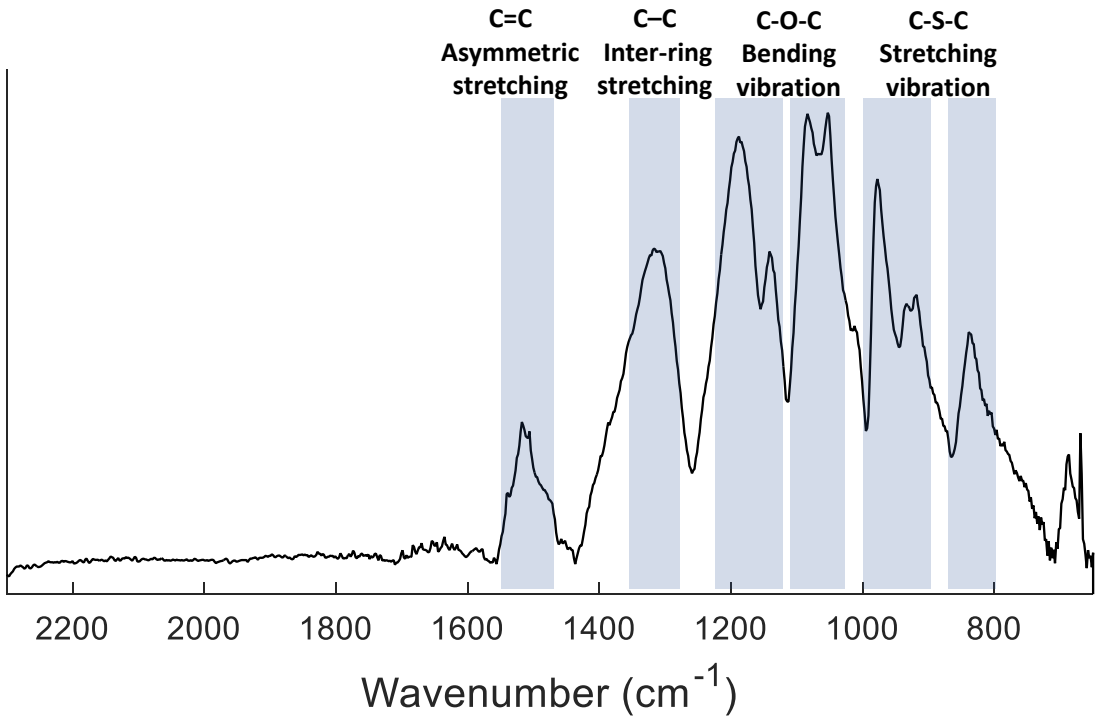

Figure 3.2 FTIR spectrum of oCVD PEDOT films.

3.3.2 Initiated chemical vapor deposition (iCVD) of PDVB Deposition

A 100 nm thick blocking layer of the electrically insulating polymer poly (divinylbenzene) (PDVB), was also deposited by CVD. This electrically insulating layer is necessary to accurately measure the thermal conductivity of electrically conductive materials using the 3ω method. Typically, processes such as sputtering or physical vapor deposition are used to deposit an electrically insulating layer such as silicon dioxide, however, sputtering may damage the polymer film and the high temperature involved will also be detrimental. In

contrast, CVD polymerization of PDVB requires low substrate temperature (20 ˚C to 70 ˚C) and does not damage the PEDOT layer.

The monomer divinylbenzene (DVB) and initiator TBPO were purchased from Sigma-Aldrich and used without further purification. Details about the iCVD polymerization of PDVB have been reported previously[39], and the deposition conditions are summarized in Table 3.3. Briefly, DVB was heated in a stainless-steel jar at 65 °C and its vapors along with vapors of tert-butyl peroxide (TBPO) (at room temperature) were delivered into the reactor at flow rates of 2.0 sccm and 1.3 sccm, respectively. Argon gas was also introduced into the reactor at 8.5 sccm. The labile peroxide bond of the initiator was thermally cleaved by resistively heated nichrome filaments inside the CVD reactor to produce free radicals that attack vinyl bonds on DVB and initiate free-radical polymerization. iCVD is a substrate-independent process as the substrate temperature remains close to room temperature. Here, the reactor pressure, substrate temperature, and filament temperature were maintained at 500 mT, 25 °C, 230 °C, respectively. A schematic of the iCVD reactor is shown in Figure 3.3.

Table 3.3 Summary of iCVD PDVB parameters

Substrate temperature (°C)	25
Filament temperature (°C)	230
Reactor pressure (mT)	500
Initiator flow rate (sccm)	2.0
Monomer flow rate (sccm)	1.3
Argon flow rate (sccm)	8.5
*** P_m/P_{sat}**	0.14

* P_m is the partial pressure of monomer inside chamber, P_{sat} is the saturation pressure of monomer on the substrate. P_m/P_{sat} can be viewed as a direct measure of monomer surface concentration on the substrate.

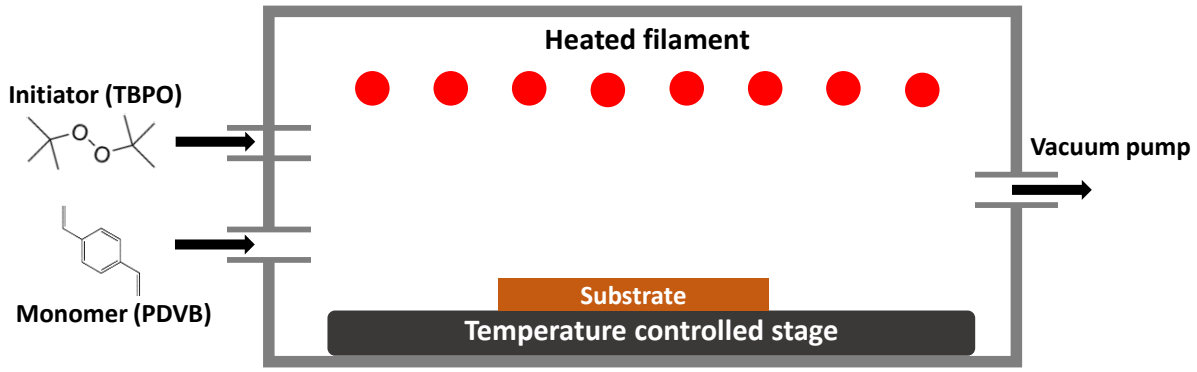

Figure 3.3 Schematic of iCVD reactor. A heated jar is used to introduce the monomer vapor into the reactor. The volatile initiator is introduced at room temperature and decomposes into free radical by the heated filament. These free radicals initiate free-radical polymerization with the vinyl bonds on DVB.

3.3.3 Scanning Electron Microscopy (SEM) on trench sample

Cross-sectional scanning electron microscopy (SEM) was utilized to check conformality and verify thickness measurements for PEDOT films. Sample cross sections were prepared by cutting samples using a diamond tipped pen. Images were recorded using an FEI Quanta 600 FEG SEM operating in secondary electron mode, with an

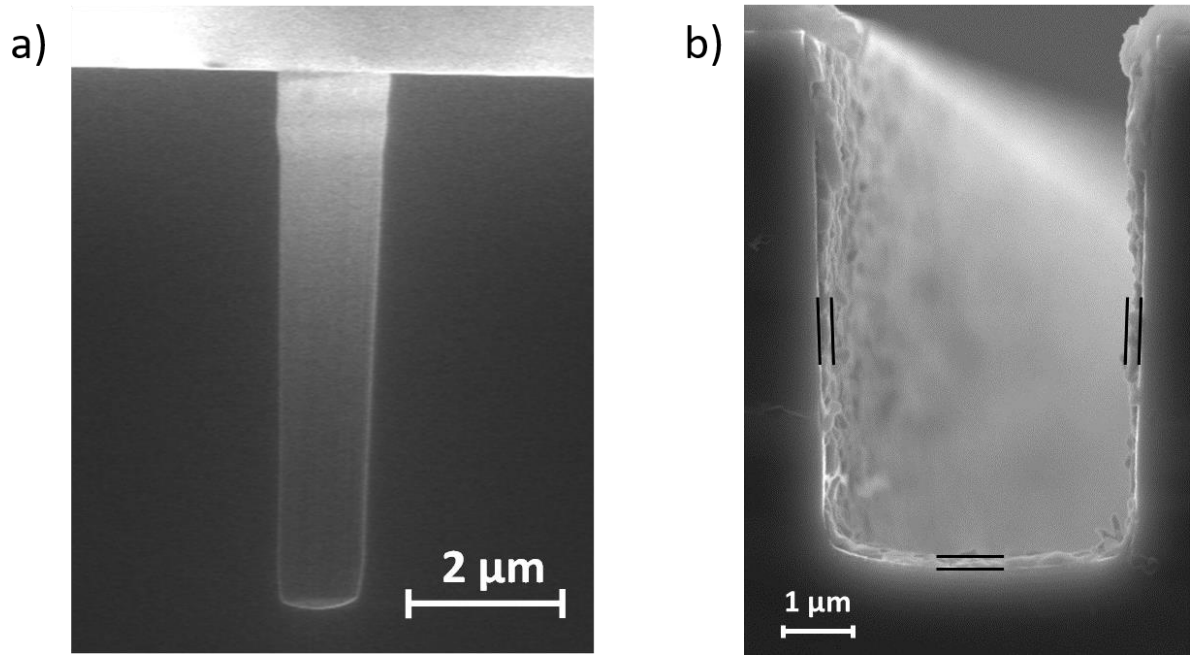

Figure 3.4 Cross-sectional SEM of a) plain trench without polymer coating b) oCVD grown PEDOT

accelerating voltage of 10 kV and a spot size of 3. An image of a plain and a coated trench is shown in Figure 3.4

3.3.4 3ω method and transmission line method (TLM)

The thermal conductivity was measured following the procedure discussed in *Chapter 2.2 The 3ω Method*. Specifically, the differential 3ω technique was chosen because (a) knowledge of the thermal properties of the substrate and other materials deposited on the substrate are not required, and (b) the error associated with the differential 3ω method has been shown to be less than that of the slope-based 3ω method[25]. Temperature dependent thermal conductivity measurements were restricted to between 160 K – 300 K due to experimental constraints. It should be noted that the thermal conductivity obtained is the effective thermal conductivity because it includes interface thermal resistance.

For the TLM measurements, the same sample preparation technique was used as outlined in *Chapter 2.2.3 Sample Preparation* except for using a different mask pattern and using multiple masks. A mask was first placed on the substrate before oCVD deposition to pattern the PEDOT film. Another mask was then placed on top of the first for electrode deposition. Gold electrodes with varying spacing between pairs of electrodes were then deposited using e-beam evaporation. 4-point resistance measurements were done between each pair of electrodes. The total resistance (R_T) between two contacts is given as

$$R_T = \frac{R_s}{W} L + 2R_c, \qquad R_s = \frac{1}{\sigma\, t} \tag{3. 1}$$

where R_s is the sheet resistance, L is the spacing between two electrodes, W is the width of the electrode, σ is the electrical conductivity and t is the film thickness. The electrical conductivity is then calculated from the slope of the total resistance as a function of electrode spacing [40]. Figure 3.5 shows results for the oCVD PEDOT film deposited at a stage temperature of 100 ˚C, where the measured resistance is plotted as a function of electrode spacing. The insert in Figure 3.5 shows the gold electrodes on the PEDOT film with conductive epoxy and bonded wires.

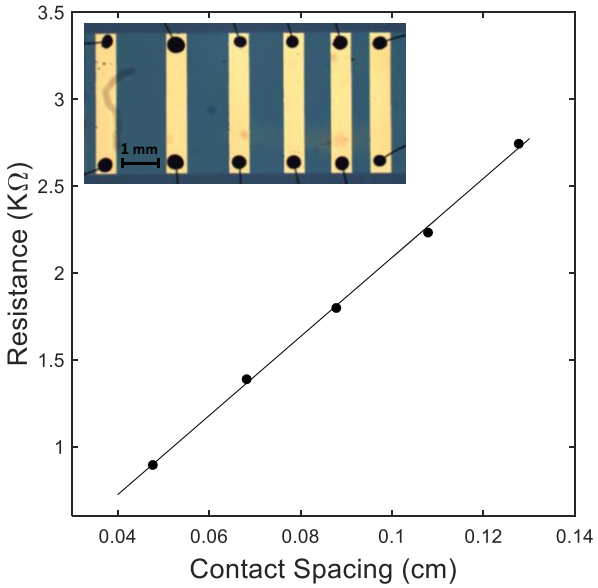

Figure 3.5 Resistance vs contact spacing of oCVD PEDOT film grown at a substrate temperature of 100 ˚C. Insert is an optical image of metal contacts with different spacing between pairs of electrodes

3.4 Results and Discussion

Figure 3.6 shows that the thermal conductivity of oCVD grown PEDOT films increases with temperature. A similar behavior has also been observed from the conducting polymer polyaniline within the same temperature range[30]. This occurs because of the thermal conductivity's dependence on heat capacity in the measured temperature range[41]. This trend is seen in polymers deposited at all three substrate temperatures.

Table 3.3 summarizes thermal and electrical conductivity values measured at room temperature for PEDOT films deposited at 70 ˚C, 100 ˚C and 130 ˚C, with 130 ˚C being the upper limit of the oCVD system. From the data, a clear correlation between electrical conductivity and substrate temperature is observed. This behavior is due to an increase in the conjugation length of the PEDOT film with elevated substrate temperature, which can be directly correlated to an increase in electrical conductivity[38]. Comparing the films

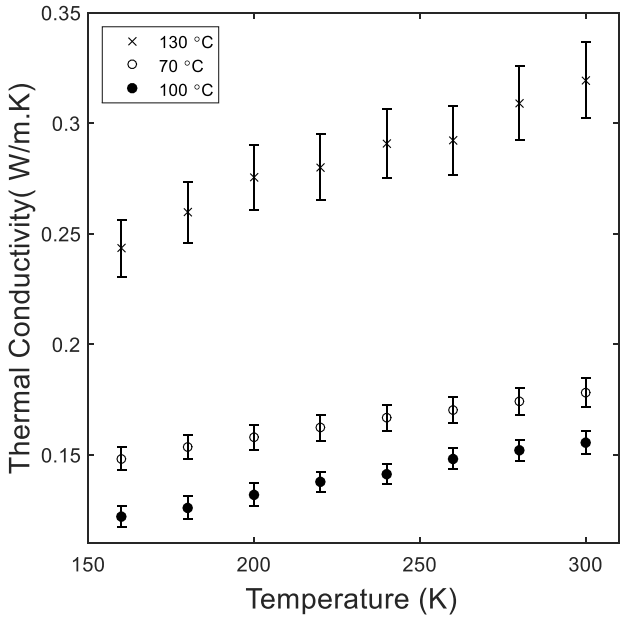

Figure 3. 6 Temperature dependent thermal conductivity of oCVD PEDOT grown at substrate temperatures of 70 ˚C, 100 ˚C and 130 ˚C

deposited at 70 ˚C and 100 ˚C, we observe an order of magnitude increase in the electrical conductivity. However, a further increase in the substrate temperature to 130 ˚C only results in a 20% increase in film electrical conductivity. One explanation for this result is the formation of hydrogen chloride (HCl) during the polymerization[38]. During the step growth polymerization of EDOT with $FeCl_3$, the acidic HCl formed acts as an inhibitor, and reduces the film's electrical conductivity. At a higher substrate temperature, the HCl content is reduced, resulting in a higher electrically conductive film. Nevertheless, it appears that a saturation point was attained in our system after which only a moderate increase in conductivity is observed with increasing substrate temperature. Also, based on the small phonon mean free path (< 10 nm) of amorphous polymers[41], the effect of phonon boundary scattering is not expected to be seen in films with the thicknesses reported here.

From the room temperature values shown in Table 3.4, no clear correlation between thermal and electrical conductivity can be deduced at these electrical conductivity values. The thermal conductivity of solution processed PEDOT:PSS typically falls within the ranges of 0.3 to 2.2 W/m·K[42][43]. However, as seen in Table 3.4, oCVD PEDOT films can attain lower thermal conductivities at room temperature. One possibility is due to the absence of PSS. A large fraction of the covalent bonds present in PEDOT:PSS is contributed by the relatively large PSS molecule. Compared to van der Waals bonds, these stiff covalent bonds are more effective at transferring thermal energy between polymer chains[44]. This suggests that PEDOT films synthesized without PSS could have predominately van der Waals bonds allowing for lower thermal conductivity.

3.5 Conclusion

The common trend in studies geared towards improving the figure of merit in PEDOT:PSS based thermoelectric materials is the reduction or removal of the insulating PSS molecule[42,43]. Reproducibility of results may also be an issue with solution processed materials. The highly scalable oCVD PEDOT films are interesting in this regard because they are PSS free and the compositions and thicknesses of these nanoscale films are reproducible[10][45]. The all vapor CVD technique also facilitates the creation of

Table 3.4 Room temperature thermal and electrical conductivities of oCVD PEDOT film deposited at different substrate temperatures.

Stage Temperature [˚C]	70	100	130
Film Thickness [nm]	95	64	53
Thermal Conductivity [W/m·K]	0.185	0.156	0.319
Electrical Conductivity [S/cm]	1.79	18.60	22.26

conformal films on textured substrates. From this study, we conclude that in oCVD PEDOT films with electrical conductivities ranging from 1 S/cm to 30 S/cm, the electronic contribution to the thermal conductivity is minimal and that phonon transport is dominant. Our thermal measurements thus provide evidence that CVD polymerization is a promising new approach to engineer PEDOT thin films which combine low thermal conductivity with relatively high electrical conductivity values. Furthermore, the highly tunable nature of this CVD technique opens opportunities for precisely tailoring the chemical composition, morphology, and electrical and thermal conductivities of polymer films to meet specific device/application requirements. This will be beneficial to many areas such as thermoelectric generators, photovoltaics, and lithium ion batteries.

Chapter 4: Morphological and Molecular Control of oCVD Polythiophene Thin Films

4.1 Introduction

Unique and cost effect avenues are constantly being explored especially in the ever-growing semiconductor industry. Organic semiconductors have become the main area of research for many industrial and academic institutions. They are light weight, mechanically flexible and have low fabrication costs. Common technologies are constantly integrating organic semiconductors to take advantage of their unique properties such as organic thin film transistors, organic solar cells and organic light emitting diodes (OLEDS)[46]. The major advancements that have been done in the field of organic electronics is expected to increase the market size from $46.12 billion in 2019 to $159.11 billion by 2027[47]. Unsubstituted polythiophene is an important semiconducting polymer because of its simple structure, optoelectronic properties, and high stability[48]. Also, from a thermal standpoint, unsubstituted polythiophene has better transport properties compared to its derivates. For example, polythiophene derivatives with oxygen atoms would have lower thermal conductivity since the heavier oxygen atoms can reduce phonon group velocity[49].

Majority of the work being done has been using substituted polythiophene such as poly(3,4-ethylenedioxythiophene) (PEDOT) and poly(3-hexylthiophene) (P3HT) because of the solubility of their monomers and ease of processing. The insolubility of unsubstituted polythiophene limits its applications as an active layer in devices. Electrochemical polymerization provides an opportunity for depositing polythiophene however the substrate requirements is strict in that it must be electrically conducting.

Another method is by a simple heat treatment, the spin-coated polymer poly-(3-(2-methylhexan-2-yl)-oxy-carbonyldithiophene) (P3MHOCT), can be converted to unsubstituted PT[48]. Oxidative chemical vapor deposition (oCVD) is a solvent free technique where all the reactants are in the vapor phase allowing for the deposition of insoluble polymers.

Although unsubstituted polythiophene has been deposited with oCVD, in one case the oxidant used was vanadium oxytrichloride which is a liquid oxidant[50] and not the most common oxidant used in oCVD. oCVD PT films deposited using iron (III) chloride ($FeCl_3$) as the oxidant has been demonstrated[13,51], however, very large monomer flow rates (~31 sccm) are used. Such a high flow rates are not easily obtained in systems outside the authors institution. Here, the oCVD synthesis of unsubstituted polythiophene using iron (III) chloride ($FeCl_3$) is reported. Raman spectroscopy and scanning electron microscopy are used to characterize the deposited PT films. By controlling the synthesis parameters, characteristics such as morphology and transport properties can be tuned.

4.2 Methods

The general procedure for depositing PT thin films is similar to that of poly(3,4-ethylenedioxythiophene) (PEDOT) reported in the previous chapter[32]. The monomer, thiophene, is placed in a heated stainless-steel jar. However, unlike the monomer 3,4-ethylenedioxythiophene (EDOT) which was heated to 130 ˚C, thiophene was heated to a lower temperature. Since thiophene has larger a vapor pressure than EDOT, heating is not necessary to create vapors. In this case, thiophene was heated to a constant temperature of 30 ˚C to avoid changes in flow rate due to fluctuating room temperature. The oxidant, iron (III) chloride ($FeCl_3$), was heated in a crucible at 180 ˚C and the Argon

flow rate was kept at 1 sccm. In the optimization process, the pressure, monomer flow rate and stage temperature were tuned. The polymerization proceeds via step-growth polymerization described in chapter 2.1[17]. The resulting film deposited on a glass slide is shown in Figure 4.1. The dark color suggests that $FeCl_3$ is still present, doping the film. A post deposition rinse in methanol for 5 mins de-dopes the film causing a change in color to a light orange.

Raman spectra was taken with a NT-MDT Raman microscope with a 532 nm laser. Figure 4.2 shows the Raman spectra of oCVD PT as-deposited and after methanol rinse. In the range of 1300 cm^{-1} – 1600 cm^{-1}, the strongest peak seen at 1461 cm^{-1} is assigned to the C=C symmetric stretching mode. The weak peak seen at ~ 1502 cm^{-1} is assigned to the C=C anti symmetric stretching mode. A shift to lower wavenumber and a decrease in intensity has be correlated to a higher conjugation length[52]. The peak at 1365 cm^{-1} is assigned to the C_β-C_β' vibration in the thiophene ring and is weak in the rinsed sample. In the range of 1000 cm^{-1} – 1250 cm^{-1}, the strongest peak at 1049 cm^{-1} is attributed to the C-H bending mode. The peaks at 1222 cm^{-1} and 1152 cm^{-1} are attributed to C_α-C_α' vibration and inter chain C-C stretching bands, respectively. It should be noted that broadening of the width of the bands are indicative of induced doping in the PT films. This provided evidence that the deposited film was polythiophene and that rinsing in methanol de-doped the films. Raman was used to verify each sample mentioned below after deposition.

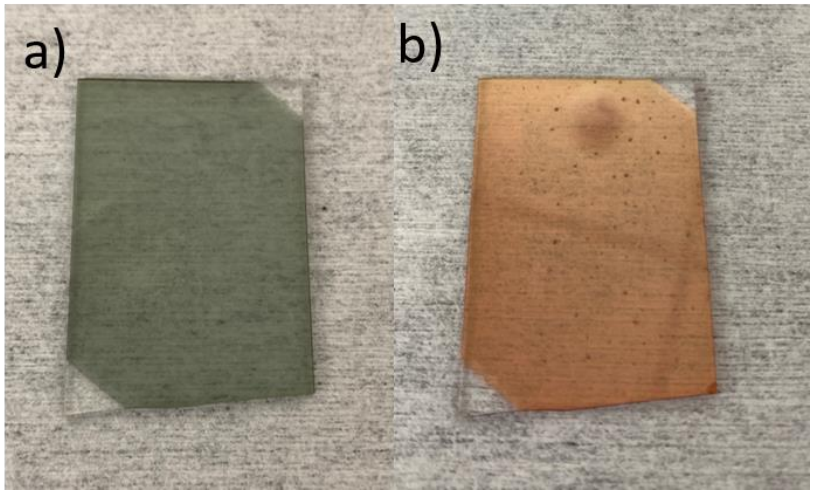

Figure 4.1 oCVD PT film on glass slide: a) As-deposited (b) after methanol rinse. The darker film is doped with the oxidant $FeCl_3$ whereas the light orange film is de-doped and is not conducting.

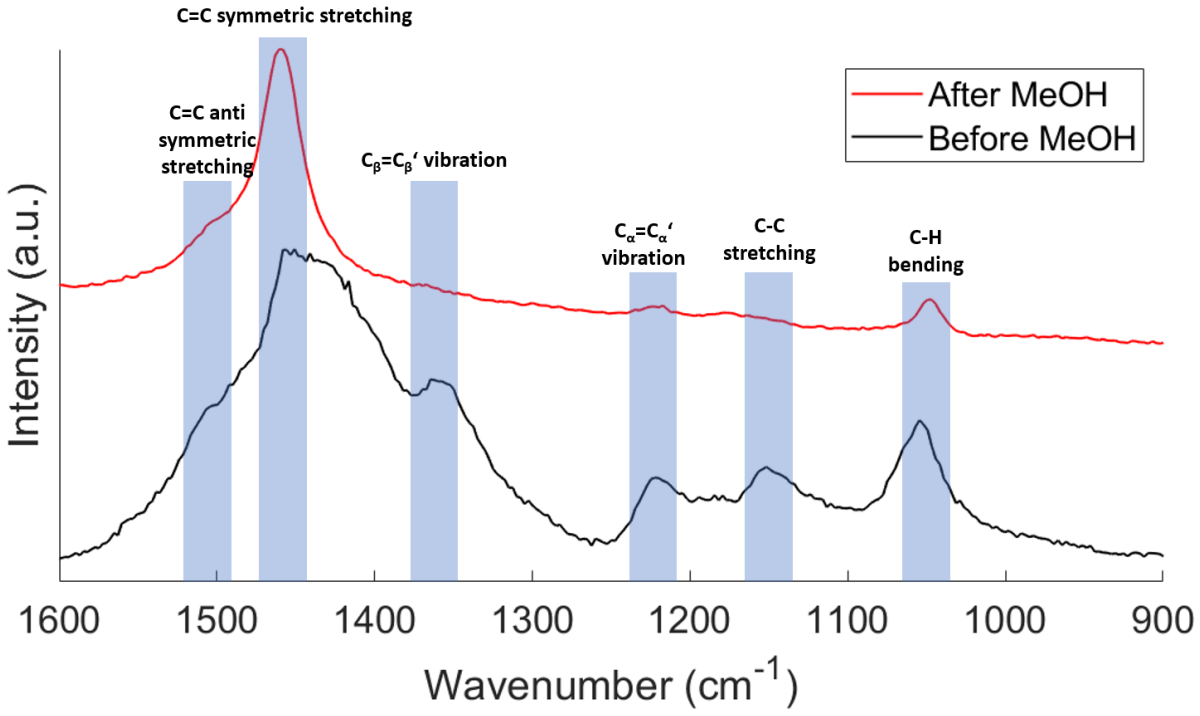

Figure 4.2 Raman spectra of oCVD PT as-deposited and after methanol rinse.

4.3 Results and Discussion

All the tunable parameters on the oCVD system are shown in figure 4.3. When optimizing the growth parameters for polythiophene, not all parameters were adjusted. As mentioned earlier, heating the monomer to a high temperature to create vapors is not necessary. However, a constant temperature of 30 ˚C was used to avoid changes in flow rate due to fluctuating room temperature. The monomer line and manifold were both heated to 60 ˚C to prevent condensation in the line. The chamber temperature was set to 60 ˚C to minimize polymer deposition on the chamber walls. The oxidant heating temperature was kept fixed at 180 ˚C. This temperature was obtained from the PEDOT growth recipe development. The parameters that are adjusted are the stage temperature, monomer flow rate and deposition pressure. It should be noted that a needle valve was used to set the monomer flow rate, as a result it was difficult to fix flow rates between depositions. Typically, when optimizing CVD processes, the ratio of the partial pressure and the saturation pressure of the monomer needs to be determined. However, since the flow rate of the oxidant is difficult estimate, this approach could not be used. Instead, parameters were adjusted based on observation of the resulting film.

Initial values for deposition parameters were taken from literature[13,51]. However, since not all CVD reactors are built the same, the exact values reported could not be used. Figure 4.4 (a) shows an SEM image of a sample deposited using the following

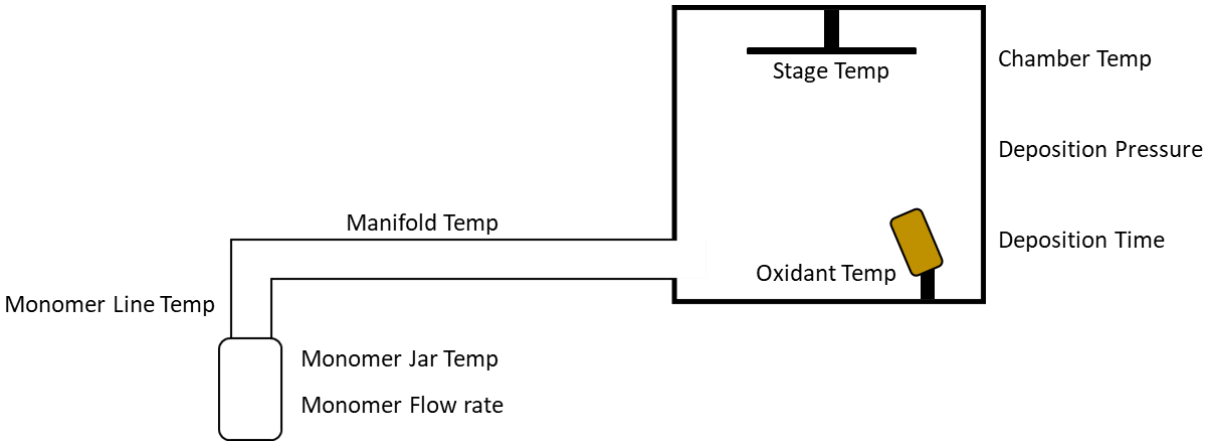

Figure 4.3 Schematic of tunable parameters on the oCVD system.

parameters, monomer flow rate: 0.71 sccm, stage temperature: 30℃ and deposition pressure: 26 mT. The resulting PT film was not continuous but more like small islands. This could be attributed to the small amount of monomer being adsorbed onto the substrate. To improve this, the monomer flow rate and the stage temperature were adjusted. First the monomer flow rate was increased to 2.13 sccm while keeping other parameters from the sample in figure 4.4 (a) fixed. The resulting sample shown in figure 4.4 (b) was very porous and again a continuous film was not obtained. Next the stage temperature was decreased to 10℃ which is the lower limit of our system while keeping other parameters from the sample in figure 4.4 (a) fixed. The resulting sample shown in figure 4.4 (c) is a continuous film, however, from the SEM image the film appears non-uniform. This suggests that further optimization is necessary.

The substrate temperature was fixed at 10℃ since a continuous film was obtained. Figure 4.5 (a) is the same as figure 4.4 (c). To improve the uniformity, the monomer flow rate and the deposition pressure were adjusted. First the monomer flow rate was increased to 4.90 sccm while keeping other parameters from the sample in figure 4.5 (a) fixed. The SEM image in figure 4.5 (b) revealed that small holes/voids were formed in the film. One

observation made during the depositions was that the deposition pressure affects the oxidant evaporation rate. This could explain the SEM image shown in figure 4.5 (C) where the film appears to be continuous and uniform.

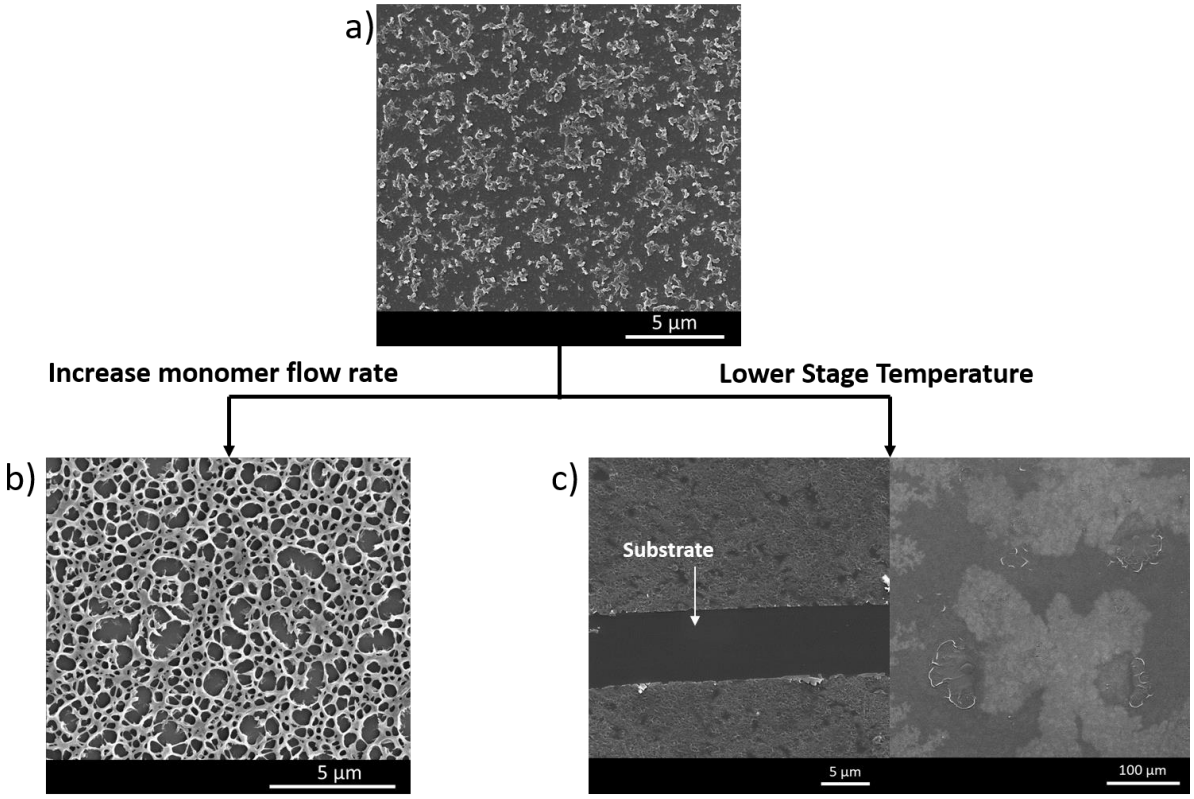

Figure 4.4 SEM images of samples showing the effect of monomer flow rate and stage temperature. In (a), the deposition was done at a monomer flow rate of 0.71 sccm, pressure of 26 mT and stage temperature of 30℃. In (b) the monomer flow rate from (a) was changed to 2.13 sccm while all other parameters were kept constant. In (c) the stage temperature from (a) was changed to 10℃ while all other parameters were kept constant.

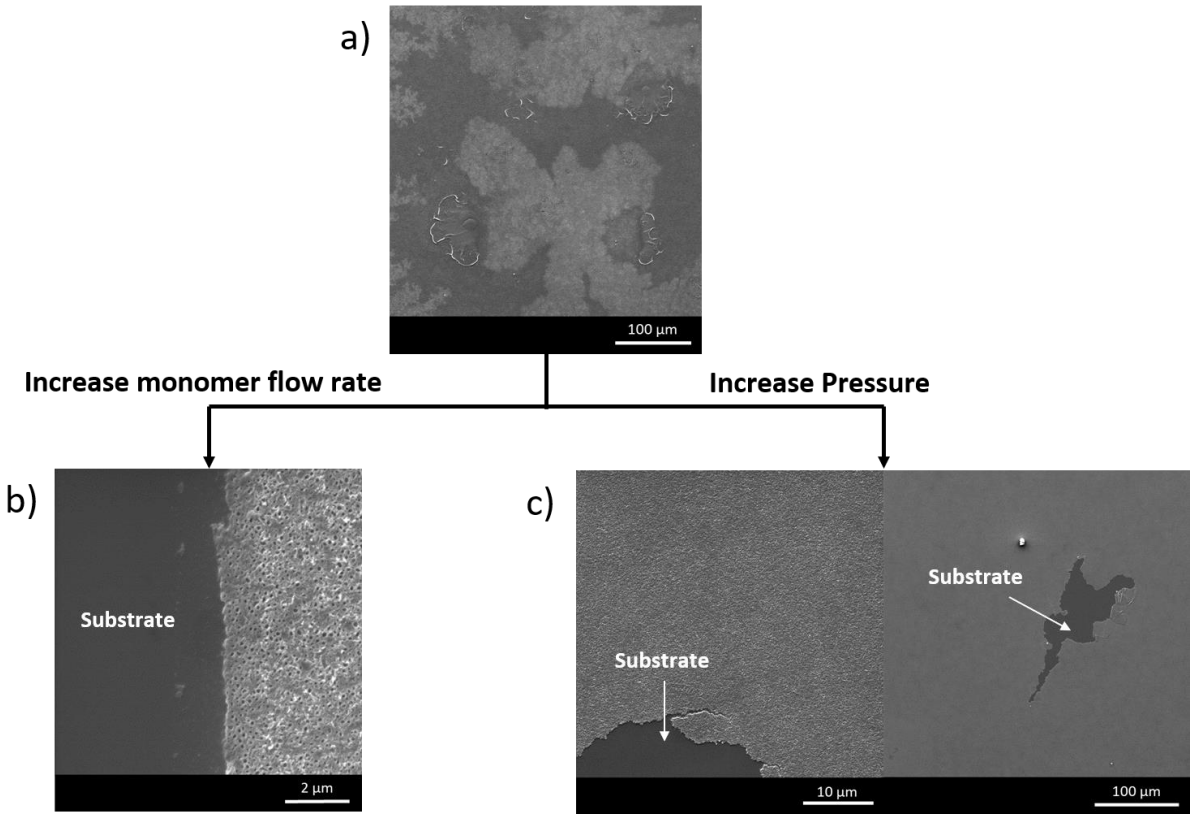

Figure 4.5 SEM images of samples showing the effect of monomer flow rate and deposition pressure. (a) corresponds to figure 4.4 (c) where the stage temperature was 10 ℃, the monomer flow rate was 0.63 sccm and the pressure was 26 mT. In (b), the monomer flow rate was increased to 4.90 sccm while all other parameters were kept constant. In (c), the deposition pressure from (a) was increased to 50 mT while all other parameters were kept constant.

4.4 Conclusion

The deposition of thin films of polythiophene has been demonstrated using iron chloride as the oxidant and relatively low monomer flow rates. Changes in the morphology of the films were observed during the optimization. This was most likely due to the large vapor pressure of thiophene compared to EDOT, making it difficult for the monomer to adsorb onto the substrate surface. Raman spectroscopy provided evidence that the deposited film was unsubstituted polythiophene. From the SEM images we concluded that the lowest temperature is best for improving monomer adsorption, the optimal monomer flow rate is between 1 – 2.5 sccm and the oxidant evaporation is dependent on the deposition

pressure. The future direction for this work would be to determine how these different morphologies affect the electrical and thermal properties of the film.

Chapter 5: Isolating specific vs non-specific binding responses from PEDOT based Chemiresistive Biosensors

5.1 Abstract

A longstanding challenge for accurate sensing of biomolecules such as proteins, concerns specifically detecting a target analyte in a complex sample (e.g., food) without suffering from non-specific binding or interactions from the target itself or other analytes present in the sample. Every sensor suffers from this fundamental drawback, which limits its sensitivity, specificity, and longevity. Existing efforts to improve signal-to-noise ratio involve introducing additional steps to reduce non-specific binding, which increases the cost of the sensor. Conducting polymer-based chemiresistive biosensors can be mechanically flexible, are inexpensive, label free and capable of detecting specific biomolecules in complex samples without purification steps, making them very versatile. In this paper, a poly (3,4-ethylenedioxyphene) (PEDOT) and poly (3-thiopheneethanol) (3TE) interpenetrating network on polypropylene-cellulose fabric is used as a platform for a chemiresistive biosensor, and the specific and non-specific binding events are studied using the Biotin/Avidin and Gliadin/G12 specific complementary binding pairs. We observed that specific binding between these pairs results in a resistance drop with the addition of the analyte and this response increases with increasing analyte concentration. Non-specific binding was found to have the opposite response, an increased resistance upon the addition of analyte was seen in non-specific binding cases. We further demonstrate the ability of the sensor to detect a targeted protein in a dual protein analyte solution. The machine learning classifier, random forest, predicted the presence of biotin with 75% accuracy in dual analyte solutions. This capability of distinguishing between

specific and non-specific binding can be a step towards solving the problem of false positives or false negatives to which all biosensors are susceptible.

5.2 Introduction

From the ever growing need to detect different biomolecules such as proteins or enzymes, the advancement of biosensing technology has become an interdisciplinary area of research bringing together biologists, physicists, chemists and engineers. The medical field, food industry and environmental monitoring are a few areas where biosensors are utilized[53]. A typical biosensor consists of the detected analyte, a bioreceptor which binds specifically to the detected analyte and a transducer which converts the binding event into a measurable signal [54]. Sensing platforms such as enzyme-linked immunosorbent assay (ELISA) and surface plasmon resonance (SPR), are based on immunoassays and plasmon generation, respectively. However, ELISA suffer from a relatively long sample preparation and high costs which limits it to laboratory applications[55] and SPR suffer from low sensitivity to low molecular weight molecules since it is mass sensitive[56].

All these platforms work on the principle that sensing occurs when a targeted analyte specifically attaches to a capture molecule anchored on a substrate. However, exposure to other non-targeted analytes for example, in complex samples like blood, will result in nonspecific binding events, producing a signal which obscures the signal from the analyte of interest, essentially adding noise to the measurement. Non-specific binding also occurs when the targeted analyte binds to sites other than the capture molecule. Every sensing platform suffers from this fundamental drawback, which limits its sensitivity, specificity, and longevity. Existing efforts to improve signal-to-noise ratio involve introducing steps to

reduce non-specific binding by imposing a blocking layer to shield unoccupied binding sites [57,58]. This blocking layer reduces analyte adsorption onto the unoccupied sites without interfering with the capture molecule and targeted analyte chemistries. Three main types of blocking agents used are detergent blockers, protein blockers and polymer-based blockers with each one having their own advantages and disadvantages[59,60]. Another way to improve signal to noise is to engineer materials for a sensing platform capable of detecting/distinguishing between the two binding events.

Materials that exhibit a change in electrical response due to a change in chemical environment are termed chemiresistors and sensors which utilize these materials as transducers are called chemiresistive sensors. These sensors are label-free, highly sensitive and require little to no sample preparation time[61]. Specifically, chemiresistive biosensors made from conducting polymers are low cost, operate at room temperature and can be made flexible due to the non-brittle nature of polymers. One of the major advantages of using conducting polymers is being able to modify the sensor surface with receptors to specifically target certain molecules while keeping the sensor platform the same. Poly (3,4-ethylenedioxyphene) (PEDOT) is one of the most widely used conducting polymers due to its optical transparency, mechanical flexibility, high electrical conductivity, and chemical and physical stability. It is typically copolymerized with other polymers to harness their functional groups for attaching different capture molecules. PEDOT based sensors has been used in the detection of a selective ligand for human influenza A virus (H1N1) by copolymerizing the monomer EDOT with another EDOT bearing oxylamine groups. This served as a unit for introducing sialyllactose to the side chain of the copolymer which was used in the detection of H1N1[62]. Similarly, the

copolymer, PEDOT and P3TE, deposited on a high surface area electro-spun nylon fiber mat, was used to immobilize avidin for the detection of biotin[63]. By using the high surface area substrate, a 6-fold in sensor response time was observed as opposed to a flat substrate.

Here, we use vapor phase polymerization (VPP) to deposit the polymer layer onto a high surface area polypropylene-cellulose fabric. This layer is made from the copolymerization of EDOT and 3-thiopheneethanol (3TE) into an interpenetrating network (IPN) of PEDOT and P3TE[63]. Iron (III) p-toluenesulfonate is used to polymerize EDOT, while P3TE weaves through the initially deposited PEDOT to form an IPN. This IPN structure increases interfacial area, allowing for increased binding of analyte capture molecules. This in turn increases the sensitivity of the device. Due to their high affinity to each other, the biomolecule pair of Biotin and Avidin are chosen as the analyte and capture molecules, respectively, to observe specific binding events. Gliadin, a protein found in wheat and casein, a protein found in milk are chosen to study nonspecific binding events. Machine learning classification techniques are applied to the measured response of the sensor to predict the presence of biotin with accuracies up to 75 %.

5.3 Methods

5.3.1 Vapor Phase Polymerization of PEDOT

The VPP technique used here for preparing the polymer films has been described in detail in a previous report [64]. A schematic of the VPP process is shown in figure 5.1. A polypropylene cellulose fabric was first soaked in a 40 wt% solution of $Fe(PTS)_3$ in butanol. This oxidant coated fabric was then placed in a sealed jar containing the monomer EDOT. The EDOT polymerization occurred in a furnace at 70 ˚C for 1 hour. The

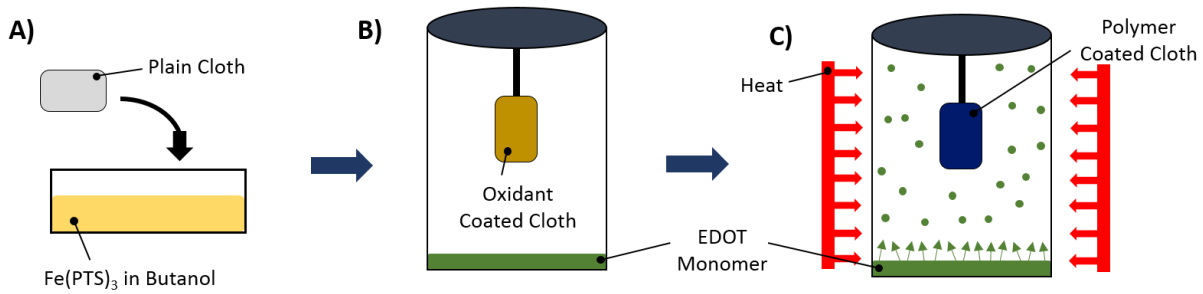

Figure 5.1 Schematic of vapor phase polymerization (VPP) process for synthesis of PEDOT films on polypropylene cellulose fabric. (a) The oxidant solution is a mixture of $Fe(PTS)_3$ in butanol. Fabric is coated by soaking in the oxidant solution. (b) The oxidant coated fabric is placed in a sealed container with the monomer. (c) Heating the container in a furnace causes the monomer to vaporize and polymerization occurs on the fabric.

PEDOT coated fabric was then rinsed in ethanol for 1 hour to remove any unreacted monomer and oxidant. The fabric was then placed in another sealed jar containing 3TE and again polymerization occurred at 70 ˚C for 1 hour.

5.3.2 Anchoring avidin to the sensor

Avidin is covalently attached to the polymer coated fabric via the linker molecule GOPS. 50 µL of GOPS was placed in a sealed contained along with the coated fabric at 120 ˚C for 2 hours. A soak in ethanol for 1 hr removed any excess GOPS molecule. Two subsequent washes in a 1:1 ratio of BSA to PBS was done for an hour each to minimize protein adsorption onto unoccupied binding sites of the sensor surface. The attachment of avidin took place overnight in a 10 mL PBS solution with 1 mg avidin.

5.4 Results and Discussion

In the VPP process, an oxidant in the liquid phase is directly deposited onto a fabric substrate. It is then exposed to the monomer vapor in a sealed container where the polymerization of the conducting polymer occurs. Typical oxidants used in this process are iron(III)chloride, copper(II)chloride and iron (III) PTS. Iron (III) PTS was chosen here

because PEDOT films produced with this oxidant has the highest reported electrical conductivity of ~ 1300 S/cm [65,66].

A schematic of the device structure is shown in figure 5.2. The capture molecules are immobilized onto the polymer surface by the functional groups of the polymer, the analyte binding to the capture molecules occurs because they have a strong affinity for each other. To immobilize the molecules responsible for capturing the analyte, linker molecules must be first bound to the conducting polymer surface. Due to the lack of appropriate functional groups, the capture molecule, in this case avidin, cannot bind directly to the polymer surface. Linker molecules such as GOPS act as a bridge between the polymer layer and the capture molecule. Figure 5.3 shows the steps taken for attachment. GOPS is a silane coupling agent which contains two different reactive groups bonded to the silicon molecule. One end of this molecule is the methoxy group while the other end is the epoxy group. The methoxy group binds with the hydroxyl group from the P3TE while the epoxy group binds to the capture molecule.

In this work, biomolecule pairs with a high affinity for each other were chosen to test the

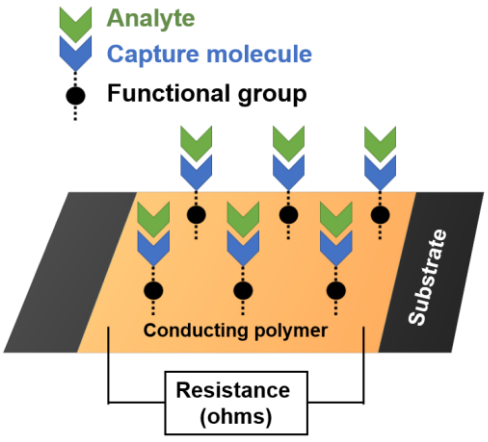

Figure 5.2 Schematic of chemiresistive sensor with capture molecule immobilization and analyte binding

response of the sensor. The first pair studied was the protein pair avidin and biotin. Avidin is a protein typically found in the egg whites while biotin is a B vitamin. The large protein avidin, can bind 4 of the small biotin molecules with dissociation constant on the order 10^{-8} s^{-1} of making it one of the strongest non-covalent bonds[67][68]. This property of the avidin/biotin pair makes them popular in western blotting[69] and in immunoassays like ELISA[70]. The other biomolecule pair is the antigen-antibody pair of G12 and gliadin. Gliadin is a class of proteins present in gluten (protein found in wheat) known to trigger reactions in Celiac patients, and its respective antibody, G12. The G12/gliadin pair has also been applied in immunoassays like ELISA [71].

FTIR was performed to check for successful growth of PEDOT and P3TE, as well as successful attachment of the GOPS molecule. FTIR was performed using a silicon wafer

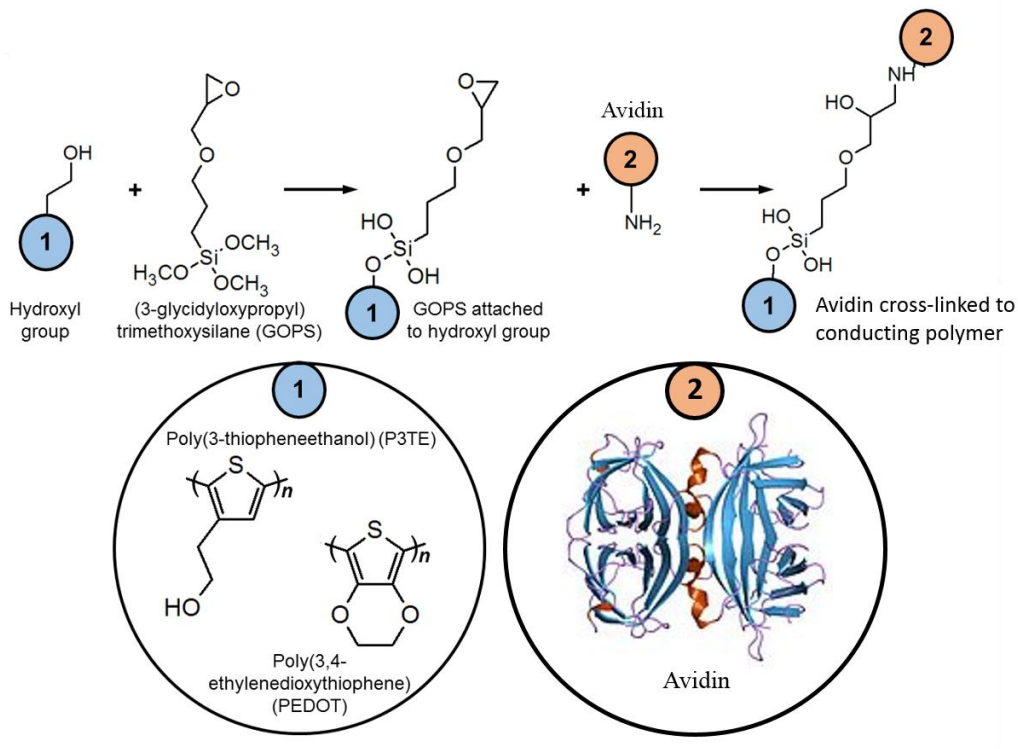

Figure 5.3 Avidin immobilization onto conducting polymer surface

as the substrate instead of the fabric. The polymer growth and GOPS attachment processes on the silicon wafer were identical to processes done on the fabric. Figure 5.4 shows the spectrum of plain PEDOT, PEDOT + P3TE and PEDOT + P3TE + GOPS. The peak correlating to the formation of the C=C in PEDOT is seen at about 1517 cm^{-1} indicating the successful polymerization of EDOT. The addition of 3TE introduces -OH functional groups which are captured in the spectrum at ~3400 cm^{-1}. Additionally, the detection of silicon (~1150 cm^{-1}) indicates the presence/successful attachment of GOPS to the interpenetrating polymer network of PEDOT and P3TE.

SEM images of the fabric substrate before and after PEDOT growth are shown in figure 5.5. Comparing the two images, the individual fibers of the fabric seen in figure 5.5b appear rougher than the ones of the uncoated fabric indicating the presence of PEDOT. It should also be noted that the morphology of the underlying fibers is retained, and that little aggregation of the polymer observed as is commonly seen during liquid-phase processes like spin coating. The retention of the fiber morphology is important because

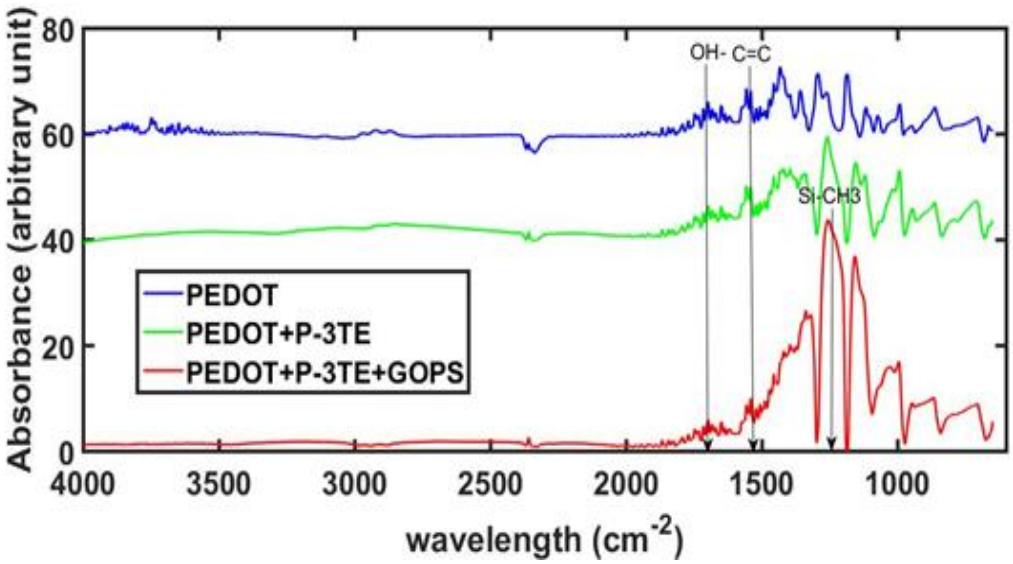

Figure 5.4 FTIR spectrum of PEDOT, PEDOT+P3TE and PEDOT+P3TE+GOPS measured on a silicon wafer

the surface to volume ratio is increased, creating more available binding sites for the analyte, increasing the ability of the sensor to detect low concentrations of the analyte.

By using a polymer-based sensor, we have the added benefit of having a low cost and mechanically flexible sensor[72]. Having such mechanical flexibility allows for manipulating these sensors in different conformations while still being able to obtain a viable signal (figure 5.6). The resulting form factor indicates that these can be easily adapted to technologies which can be embedded into clothing or worn as accessories.

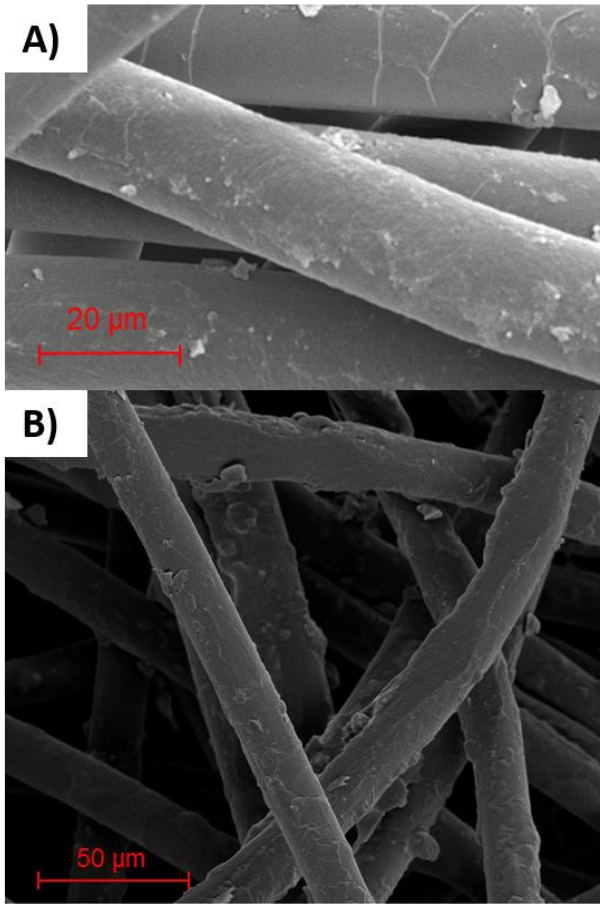

Figure 5. 5 Scanning electron microscopy of (a) uncoated fabric (b) fabric coated with PEDOT

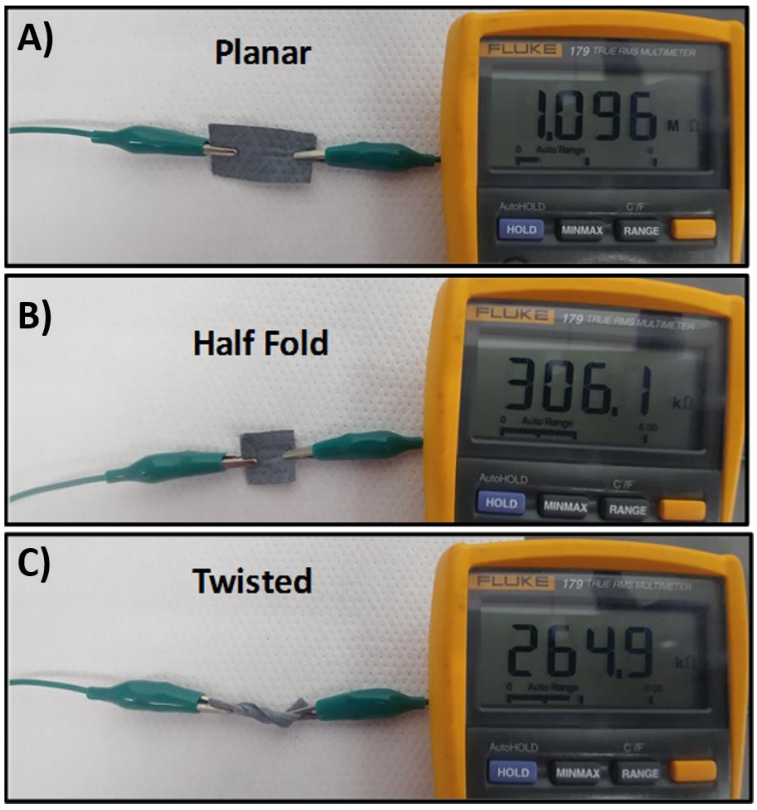

Figure 5.6 Polymer coated fabric in (a) planar (b) half fold and (c) twisted conformations.

To evaluate the response of the sensors, the electrical potential was monitored over a span of 30 mins with the analyte being added after 15 mins. The percent change in resistance is given by

$$\Delta R(\%) = \frac{R_0 - R_1}{R_1} \times 100 \qquad 5.1$$

where R_1 is the resistance before the analyte is added (at 15 mins) and R_0 is the resistance at the end of the experiment (after 30 mins). Two analytes, biotin and gliadin were tested at concentrations of 50 µM, 5 µM, 500 nM and 50 nM, each. The results showed a log-linear correlation between the concentration and the change in resistance of the sensor upon the addition of analyte (figure 5.7 (a)). At each concentration, approximately 4 identical measurements were performed which is indicated by multiple

blue circles at one specific concentration. This change in resistance was proportional to the analyte concentration indicating the ability of the sensor to provide distinguishable signals for different analyte concentrations. Furthermore, similar responses were seen for the avidin/biotin system and the G12/gliadin with the only difference being the capture molecule (figure 5.7 (b)).

Building upon these results, the next series of tests were performed to investigate the response from an analyte on a sensor with (specific binding) and without (nonspecific binding) the complementary capture molecule immobilized on the surface of the sensor. From figure 5.7 (c) there was no longer a drop in resistance as seen with complementary analyte and capture molecules, but rather an increase in resistance was observed when no capture molecule was used. These results suggest that a drop in resistance is indicative of a specific binding event whereas an increase in resistance signifies a non-specific binding event. This increase in resistance had a weak inverse correlation with the analyte concentration, which was not nearly as strong as in the case of the complementary binding pairs. Non-complementary analytes and capture molecules such as gliadin and avidin respectively, also showed this behavior. A two-way ANOVA and Tukey's pairwise test was performed, and the analysis returned a statistically significant interaction effect between whether there is a protein bound to the sensor and the analyte used. This data suggests that the non-specific binding response in our biosensors is the opposite of the specific binding response. Since similar results are seen in the data for biotin and gliadin, this tells us that the signal is solely due to the presence/absence of complementary binding pairs and not individual effects from the bound protein to the analyte. This behavior may be due to the electrical characteristics of the protein-capture

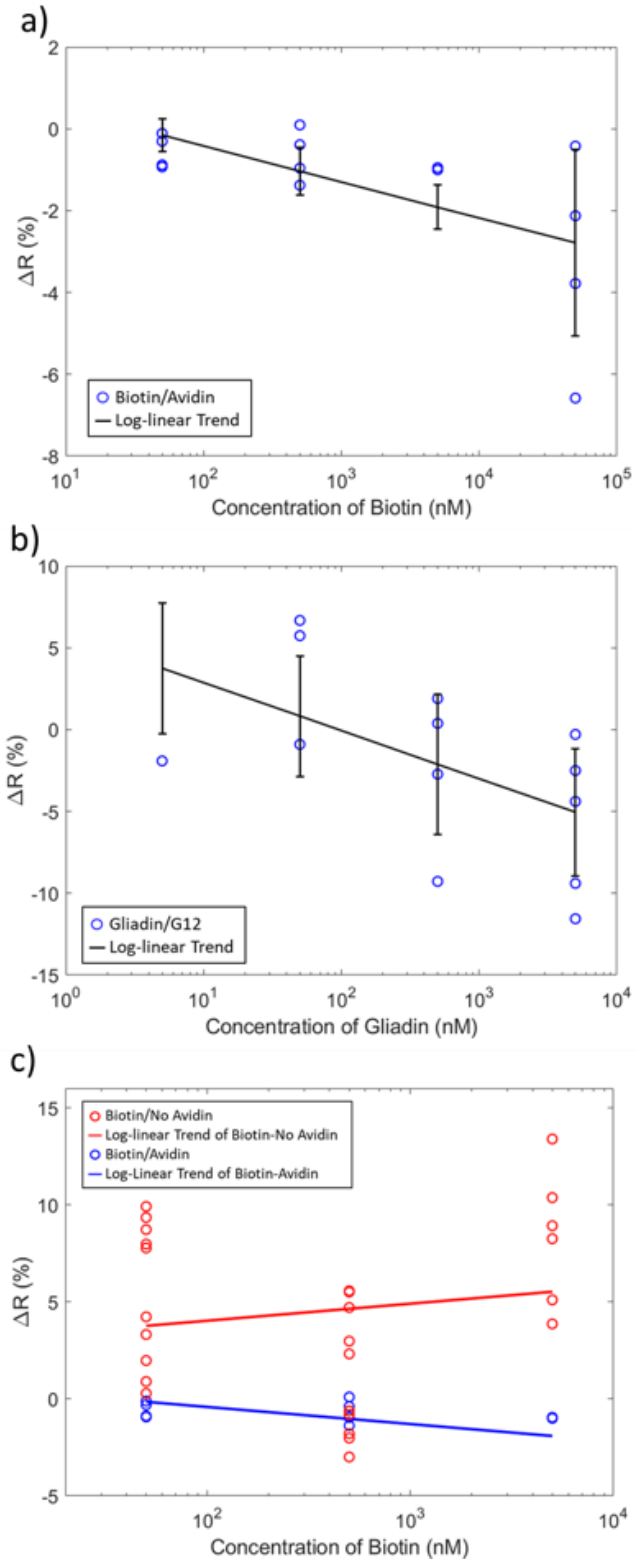

Figure 5. 7 Change in resistance vs concentration for (a) Biotin analyte with Avidin capture molecule (b) Gliadin analyte with G12 capture molecule (c) Biotin analyte with and without capture molecule

molecule bonds that occur through specific binding events. This observation can be related to gas sensors made of conducting polymer-metal hybrids. By coupling metal particles to the conducting polymer films, the change in work function experienced by the metal in the presence of a gas can be translated into changes in the electrical characteristics of the polymer film[73,74]. The sensors in this work follow a similar architecture to the gas sensor previously mentioned which suggests that the interaction between the analyte and the capture molecule is modulating the electronic properties of the polymer film.

Machine Learning Prediction

Mixed analyte solutions of casein-gliadin, biotin-gliadin and biotin-casein were also tested with the sensor immobilized with avidin (figure 5.8). Unlike the single analyte tests, the detection of Biotin cannot be inferred from a change in resistance only. Machine learning is used to build an analytical model capable of identifying patterns to predict the presence of Biotin. Four common machine learning algorithms were used to evaluate classification accuracies: support vector machines (SVM), random forest (RF), K- nearest neighbors (KNN) and logistic regression (LR). The data considered in this analysis comprised of the voltage signal after the analyte was added. The first step in our approach is the exploratory data analysis (EDA). In the EDA step, the variation of voltage with time was carefully observed and features were extracted manually from the dataset. Signal processing techniques were also applied to extract information like peak to peak difference (difference between minimum and maximum values of voltage), max signal (maximum voltage) and Kurtosis. These features were used as input to predict the presence of Biotin. The dataset was split into 80% training data and 20% test set data on

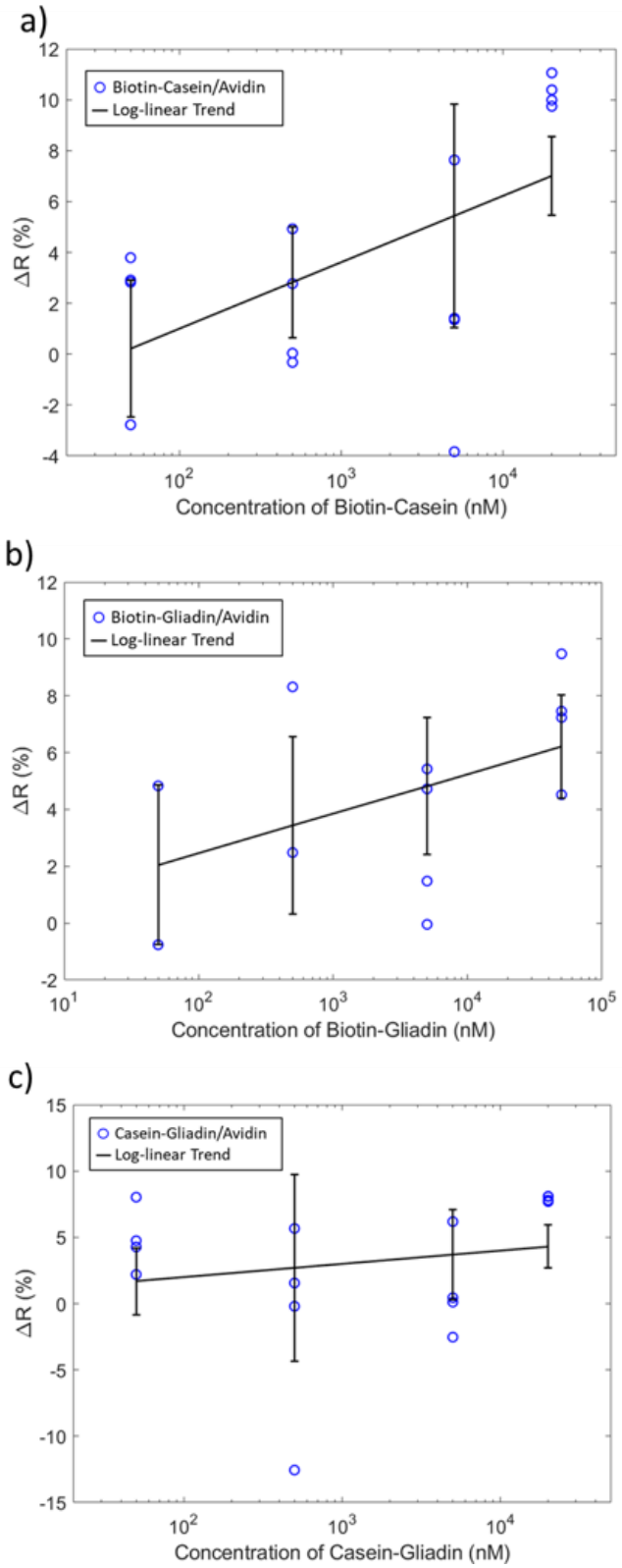

Figure 5. 8 Change in resistance vs concentration for mixed analytes all with Avidin capture molecule. (a) Biotin-Casein (b) Biotin-Gliadin (c) Casein-Gliadin

which the predictions were made. As a result, the total 73 data points were split into 58 train and 15 test datapoints. The classification accuracies range from 67% – 75% (Table 5.1) with RF performing the best out of the 4. A 5-fold cross validation was done to minimize the variance ensuring that model accuracies obtained were more reliable. RF was also used to identify the feature with the highest contribution (figure 5.9). Kurtosis yielded the highest contribution indicating that the sharpness of the peak is influenced by the presence of Biotin.

Table 5. 1 Classification Accuracies

Machine learning algorithm	Accuracy
Support Vector Machines	67 %
Random Forest	75 %
K- nearest neighbors	70 %
Logistic Regression	67 %

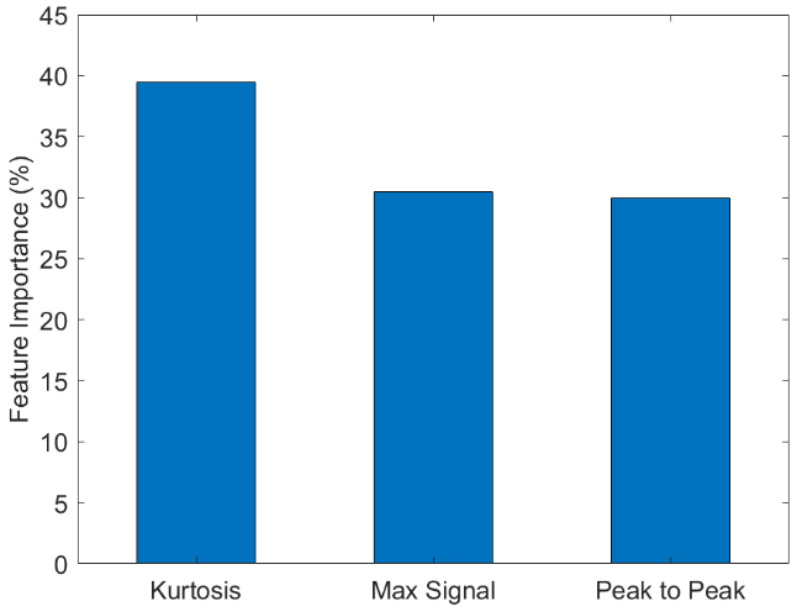

Figure 5. 9 Feature importance

5.5 Conclusion

In this study, we developed a conducting polymer based chemiresistive biosensor capable of label free sensing of biomolecules. This biosensing platform is not only capable of detecting the presence and concentration of the targeted biomolecule, but also has distinct responses to specific and non-specific binding events. When complementary analytes and capture molecules such as biotin/avidin or gliadin/G12 are measured, a drop in resistance across the sensor is seen when the analytes are added which we correlate to a specific binding event. On the other hand, when non-complementary analytes and captures molecules such as gliadin/avidin and biotin/G12 are measured an increase in resistance is observed which we correlate to nonspecific binding events. Since the same observation is made for two different sets of analytes and capture molecules, we believe that for this sensor the signal is based solely on whether the analytes and capture molecules are complementary. Furthermore, when the analyte is composed of a mixture of complementary and non-complementary molecules, the resistance is not a good measure (figure 5.8). We use a variety of machine learning algorithms to predict the presence of biotin specifically, in mixed analytes. Random forest yielded the best prediction accuracy. Different feature extraction techniques were also used to get the highest possible accuracy. Based on the feature importance of random forest, kurtosis was found to be the most important. Thus, using kurtosis as the feature and random forest as the algorithm we were able to predict the presence of biotin with accuracies up to 75%.

These results demonstrate the versality of this sensing platform for the detection of a variety of biomolecules with the use of appropriate capture molecule. Machine learning has proved useful in distinguishing different binding events making this a good candidate

for the development of ubiquitous biosensing. Such a biosensor would have a wide variety of applications, including allergen detection, monitoring circulating cancer cells in blood, and pharmaceutical drug screening.

Chapter 6: Collaborative Projects

6.1 oCVD PEDOT Thin Films Coated on Lithium Manganese Oxide Electrode

Publication[75]: Su L., Smith P. et al, ACS Appl. Mater. Interfaces 2018, 10, 27063−27073

Contribution: My contribution to this work was optimizing the growth recipe for creating a uniform and conformal PEDOT film on the particles that make up the battery electrode.

Overview

Lithium-ion batteries (LIBs) have become the choice power source for electronics such as cell phones, laptops and even electric vehicles due to their higher energy densities compared to other rechargeable systems. Current research on rechargeable lithium ion batteries are geared towards extending the lifespan, increasing energy and power density and improving safety. Poor performance of cathode material in the presence of electrolyte is a major factor limiting the overall performance of LIBs. Surface modification of the cathode electrode with an artificial solid-electrolyte interphase (SEI) layer is a widely pursued technique to enhance the overall battery performance leading to improved stability[76] and electronic and ionic conductivity of the electrodes[77]. Organic polymer coatings have been used as SEI layers previously, however, the solution processing technique used to realize the polymers offer poor control over film composition, thickness, repeatability and reliability. In this study, we utilize oCVD to deposit the conducting polymer PEDOT and initiated chemical vapor deposition (iCVD) to deposit an insulating polymer poly(divinylbenzene) (PDVB) thin film on the surface of a lithium manganese

oxide (LiMn2O4) electrode and compared their performance as artificial SEI layers. Our results show that PEDOT coatings improve both the rate and the cycling performance of LiMn2O4 electrodes, whereas insulating PDVB coatings have little effect on these performances. An 83% increase in 10 C rate capacity at 25℃ (from 23 to 43 mAh/g) is seen in figure 6.1 (a) for the PEDOT coated electrode. Furthermore, an improvement of over 40% (from 87 to 122 cycles) in the cycling life of the LiMn2O4 cell is observed from figure 6.1 (b). Results from X-ray photoelectron spectroscopy suggest that chemical or coordination bonds form between Mn in $LiMn_2O_4$ and O and S in the PEDOT film. These bonds stabilize the surface of $LiMn_2O_4$ and thus improve the cycling performance. In contrast, no bonds form between Mn and the elements in the PDVB film. This study demonstrates the potential CVD polymerization has in advancing the research into performance improvement in LIBs.

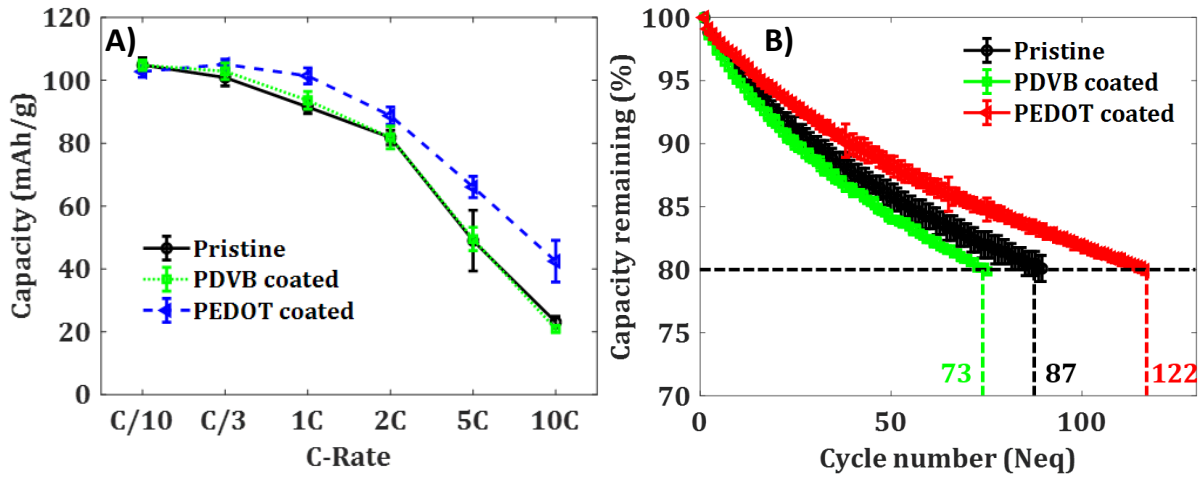

Figure 6.1 (a) Statistical data summary of cell capacities with respect to C-rates at room temperature. (b) Capacity remaining vs number of cycles

6.2 Selective and Sensitive Dopamine Sensing using 3D Fuzzy Graphene Coated with oCVD PEDOT

Publication: Submitted; In collaboration with Dr. Cohen-Karni's group

Contribution: My contribution to this work was optimizing the growth recipe for creating a uniform and conformal PEDOT film with different thickness of PEDOT on the 3D fuzzy graphene structures.

Overview

Dopamine (DA), a neurotransmitter, is involved in many cognitive processes such as voluntary movement, reward motivated behavior and attention[78]. Dysregulation of dopamine is implicated in conditions such as Parkinson's disease, addiction, and depression[79]. However, the knowledge of DA's role in such conditions is limited[80]. Sensors that can precisely determine the concentration of dopamine with high spatial and temporal specificity can help reveal the dynamics of DA regulation and dysregulation. Therefore, the development of such sensors has drawn great interest. Electrochemical techniques are often preferred due to their ease of use, low cost, and fast sampling times [81]. One of the challenges associated with the detection of DA is that DA co-exists with several electroactive species, such as uric acid (UA) and ascorbic acid (AA), with similar oxidation potentials and much higher concentrations. The presence of these species obscures the electrochemical signal of DA. Addressing challenges such as this, will facilitate the development of an ideal sensor capable of detecting DA across a wide range of concentrations in the presence of interfering species. Hybrid materials of nanocarbons such as graphene and conductive polymers, have been utilized to enable more precise

detection of DA, leveraging beneficial properties of each component such as biocompatibility, high electrical conductivity, high surface area and fast electron transfer kinetics [82]. However, these materials often present a two-dimensional (2D) topology and may lack sensitivity without the addition of functional groups, nanoparticle coating, or acid treatment. 3D surface topologies that involve out-of-plane flakes (in the case of graphene) are beneficial for sensing due to increased surface area and exposure of catalytic edge planes thus increasing selectivity and sensitivity[83]. The same effect is observed in PEDOT sensors with increased surface area[84]. Recently, synthesis of 3D out-of-plane fuzzy graphene has been demonstrated on a 3D Si-nanowire (SiNW) mesh template. Nanowire templated 3D fuzzy graphene (NT-3DFG) shows high potential for electrochemical biosensing applications due to high electrical conductivity, high electrochemical surface area, and a high density of edge defects[85]. In this study, we demonstrate selective and sensitive DA detection using a hybrid nanomaterial composed of this NT-3DFG conformally coated with different thicknesses of a PEDOT thin film. oCVD was utilized to conformally and uniformly coat these 3D structures while still preserving the structure underneath. Scanning electron microscopy (SEM) images of NT-3DFG with PEDOT coatings are shown in figure 6.2. From cyclic voltammetry (CV) scans (figure 6.3 (a)) an increase in current density is observed with increased PEDOT thickness however, faster electron transfer rate was observed with thin PEDOT compared to thick PEDOT coating. To eliminate the effects of capacitive currents, differential pulse voltammetry (DPV) was performed (figure 6.3 (b)). Thin PEDOT coating exhibit a larger DA peak current density compared to the other two samples. These results indicated that optimizing the thickness of PEDOT will play a crucial role in the sensor's performance by

maximizing the current density in CV while enhancing the DA peak in DPV. This new hybrid nanomaterials opens new avenues for next-generation lab-on-chip devices

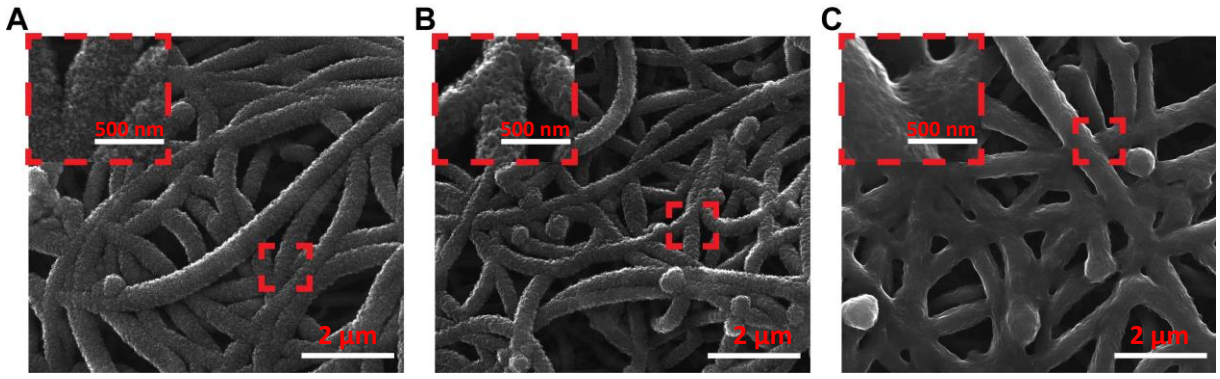

Figure 6.2 Morphological characterization of PEDOT:NT-3DFG. Representative scanning electron microscopy (SEM) image of (a) pristine NT-3DFG, (b) thin PEDOT:NT-3DFG, and (c) thick PEDOT:NT-3DFG

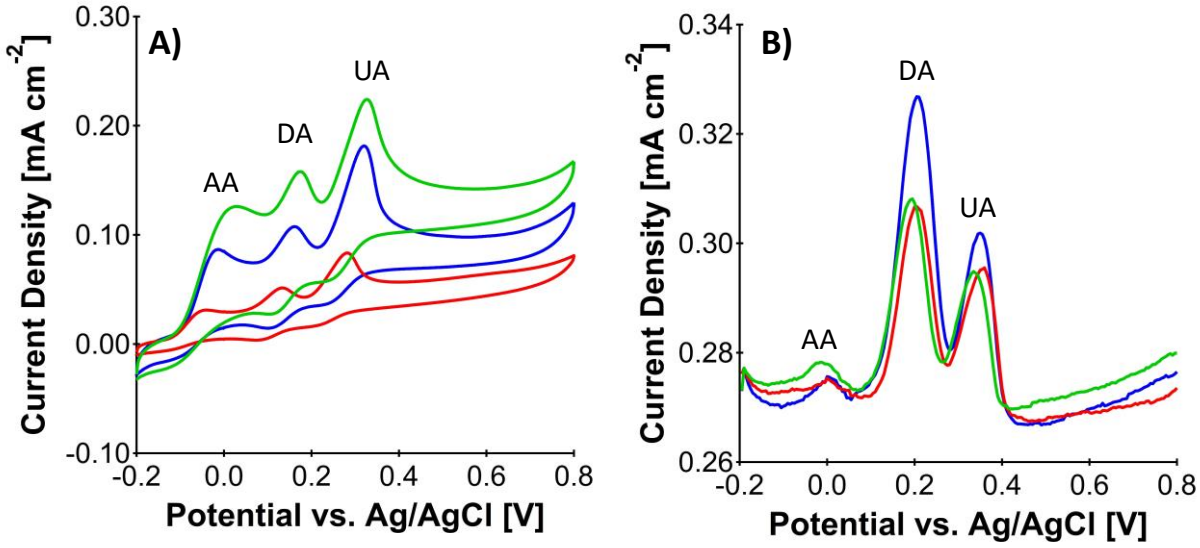

Figure 6.3 Electrochemical sensing of DA from a mixture of 1 mM AA, 500 µM UA, and 100 µM DA. (a) Cyclic voltammetry (b) Differential pulse voltammetry. Red, blue and green represent pristine NT-3DFG, patchy PEDOT:NT-3DFG, and thick PEDOT:NT-3DFG, respectively

Chapter 7: Forward Looking

7.1 Future Work

7.1.1 Thermal Conductivity Measurements

The polythiophene thin film optimization work demonstrated morphological changes in the film based on deposition parameters. There is a high probability that the films also went through structural changes. There structural changes can affect properties of the film such as optical, electrical, and thermal. Thermal transport properties are important to know especially when dealing with electronic devices which generate heat. Degradation due to high temperatures can cause failure in the electronics. Thermal transport properties like thermal conductivity can also shed like on structural changes the films may have undergone based on deposition parameters. Temperature dependent thermal conductivity will help understand electron thermal transport[41]. Also, measuring over a wide temperature range is beneficial when determining whether a material is right for your application over the working temperature range.

7.2.2 Conjugation Length Estimation

There are many factors which can affect the thermal transport in polymers including the chain structure and morphology. Longer conjugation length which corresponds to a longer chain length has been shown to improve transport properties, both thermal and electrical[50,86]. To determine a relationship between the polymer structure and thermal properties, the conjugation length should be studied with the aid of UV-vis spectroscopy.

Once the maximum absorption peak (λ_{max}) is determined via UV-vis, it can be compared to other λ_{max} from α-oligothiophenes in literature[87]. An example of λ_{max} vs number of

thiophene repeat units is shown in figure 7.1. Once λ_{max} is determined the conjugation length can be estimated.

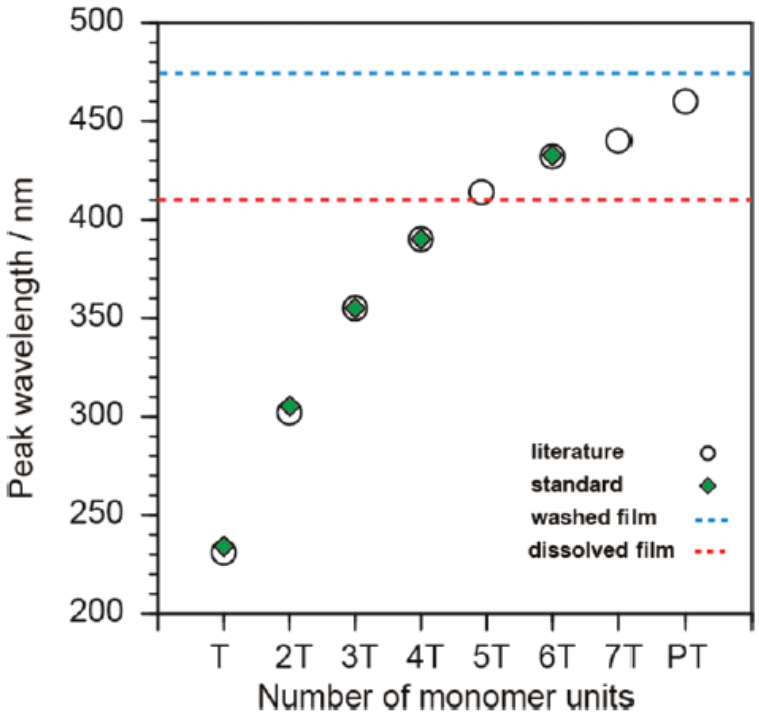

Figure 7.1 Correlation of λ_{max} from UV-Vis spectra with the number of thiophene chain units[50].

7.2 oCVD Reactor Future Improvement

The oCVD reactor used in this thesis was procured by lead PI Prof. Reeja-Jayan and was designed with future applications in mind. As mentioned earlier, there are 3 monomer feed lines which would allow for the simultaneous introduction of multiple monomers. This is important for creating copolymers with improved or modified characteristics compared to a homopolymer[73,88,89]. The system is also equipped with two thermal evaporators to allow for co-evaporation of multiple materials including the oxidant [90]. While developing the process for PEDOT and PT thin film deposition, I have identified a few

areas that can be improved upon. Further improvements to the reactor and the process can be done either by upgrading current equipment, integrating new equipment, or utilizing new materials. The possible improvements listed below originated from either a literature search or from my personal experience using the system.

7.2.1 Solid Oxidant Control

One of the major challenges with controlled film deposition is working with a solid oxidant. Accurately obtaining the flow rate of the sublimed oxidant is difficult which also makes it difficult to determine the partial pressure of the oxidant. Nonetheless, I have identified a few ways which will make working with a solid oxidant more controllable.

1. On the current system, there is no way to control the heating rate. In my experience, control over the heating rate is crucial in maintaining a uniform evaporation rate of the oxidant. Currently, the only input for the evaporator is the final heating temperature, updating the software with a field to input heating rate in addition to final temperature will provide more control over the oxidant evaporation.
2. Integrating shutters with the evaporators will help with controlling the exposure of the sample to the oxidant. During heating to desired temperature and cooling down, the shutters remain closed to avoid uncontrolled depositions. Reproducibility of film thickness among batches will be greatly improved.
3. To control the amount of oxidant that is evaporated, Xu et al. reported the use of a glass tube with a heated tungsten wire which was added on top of the evaporator to trap excessive oxidant[86].

7.2.2 In-Situ Monitoring of Film Deposition

In all film deposition techniques, the properties of the resulting film are dependent on the deposition conditions. When optimizing a process, in-situ monitoring of parameters such as deposition rates, film thickness and optical constants can significantly reduce the number of growth runs done compared to post deposition measurements. Integrating equipment like a quartz crystal microbalance (QCM)[91], an ellipsometer or an interferometer with the oCVD reactor will further improve reproducibility and reduce optimization time when a new polymer is being deposited. Furthermore, combining real-time monitoring with heating rate control, the heating power can be automatically adjusted to maintain desired deposition rate.

7.2.3 Alternative Oxidants

Oxidizing agents typically used are metal halogen salts or halogen gases[9]. Iron chloride ($FeCl_3$) is the most used oxidant but due to its low volatility, like many solid oxidants, delivery of its vapor phase to the reactor is challenging. For this reason, the oxidant is sublimed inside the reactor chamber using an evaporator. This makes it difficult to control the oxidant and determine the flow rate. These solid oxidants typically require a post deposition rinse in a polar solvent like methanol to remove excess oxidant. By switching to a more volatile oxidant, more control over the film formation can be obtained and the need for post deposition rinsing is eliminated. The oxidant would be kept outside the reactor chamber and the flow rate can be controlled using a mass flow controller (MFC) or a needle valve. Table 7.1 lists alternative oxidants found in literature that have been used in the oCVD process.

Table 7.1 List of alternative oxidants

Alternative Oxidants
Bromine [16,89]
Antimony Pentachloride [92–95]
Vanadium Oxytrichloride[95,96]

References

[1] Manning, T. D., and Parkin, I. P., 2004, “Atmospheric Pressure Chemical Vapour Deposition of Tungsten Doped Vanadium(IV) Oxide from VOCl3, Water and WCl6,” Journal of Materials Chemistry, **14**(16), pp. 2554–2559.

[2] Awang, M., Khalili, A. A., and Pedapati, S. R., 2020, “A Review: Thin Protective Coating for Wear Protection in High-Temperature Application,” Metals, **10**(1).

[3] Heeger, A. J., 2001, “Semiconducting and Metallic Polymers: The Fourth Generation of Polymeric Materials (Nobel Lecture) Copyright(c) The Nobel Foundation 2001.,” Review of Modern Physics, **73**(July), p. 681.

[4] Sun, K., Zhang, S., Li, P., Xia, Y., Zhang, X., Du, D., Isikgor, F. H., and Ouyang, J., 2015, “Review on Application of PEDOTs and PEDOT:PSS in Energy Conversion and Storage Devices,” Journal of Materials Science: Materials in Electronics, **26**(7), pp. 4438–4462.

[5] Kayser, L. v., and Lipomi, D. J., 2019, “Stretchable Conductive Polymers and Composites Based on PEDOT and PEDOT:PSS,” Advanced Materials, **31**(10), pp. 1–13.

[6] Rahman, M. A., Rahim, A., Maniruzzaman, M., Yang, K., Lee, C., Nam, H., Soh, H., and Lee, J., 2011, “ITO-Free Low-Cost Organic Solar Cells with Highly Conductive Poly(3,4 Ethylenedioxythiophene): P-Toluene Sulfonate Anodes,” Solar Energy Materials and Solar Cells, **95**(12), pp. 3573–3578.

[7] He, X., He, R., Lan, Q., Wu, W., Duan, F., Xiao, J., Zhang, M., Zeng, Q., Wu, J., and Liu, J., 2017, “Screen-Printed Fabrication of PEDOT: PSS/Silver Nanowire Composite Films for Transparent Heaters,” Materials, **10**(3).

[8] Winther-Jensen, B., and West, K., 2004, “Vapor-Phase Polymerization of 3,4-Ethylenedioxythiophene: A Route to Highly Conducting Polymer Surface Layers,” Macromolecules, **37**(12), pp. 4538–4543.

[9] Heydari Gharahcheshmeh, M., and Gleason, K. K., 2019, “Device Fabrication Based on Oxidative Chemical Vapor Deposition (OCVD) Synthesis of Conducting Polymers and Related Conjugated Organic Materials,” Advanced Materials Interfaces, **6**(1), pp. 1–27.

[10] Reeja-Jayan, B., Kovacik, P., Yang, R., Sojoudi, H., Ugur, A., Kim, D. H., Petruczok, C. D., Wang, X., Liu, A., and Gleason, K. K., 2014, “A Route Towards Sustainability Through Engineered Polymeric Interfaces,” Advanced Materials Interfaces, **1**(4), pp. 1–30.

[11] Vitoratos, E., Sakkopoulos, S., Dalas, E., Paliatsas, N., Karageorgopoulos, D., Petraki, F., Kennou, S., and Choulis, S. A., 2009, “Thermal Degradation Mechanisms of PEDOT:PSS,” Organic Electronics, **10**(1), pp. 61–66.

[12] Carlsson, J.-O., and Martin, P. M., 2010, “Chemical Vapor Deposition,” *Handbook of Deposition Technologies for Films and Coatings*, Elsevier, pp. 314–363.

[13] Borrelli, D. C., Lee, S., and Gleason, K. K., 2014, “Optoelectronic Properties of Polythiophene Thin Films and Organic TFTs Fabricated by Oxidative Chemical Vapor Deposition,” Journal of Materials Chemistry C, **2**(35), pp. 7223–7231.

[14] Gleason, K. K., ed., 2015, *CVD Polymers*, Wiley-VCH Verlag GmbH & Co. KGaA, Weinheim, Germany.

[15] Ozaydin-Ince, G., and Gleason, K. K., 2010, “Tunable Conformality of Polymer Coatings on High Aspect Ratio Features,” Chemical Vapor Deposition, **16**(1–3), pp. 100–105.

[16] Chelawat, H., Vaddiraju, S., and Gleason, K., 2010, “Conformal, Conducting Poly(3,4-Ethylenedioxythiophene) Thin Films Deposited Using Bromine as the Oxidant in a Completely Dry Oxidative Chemical Vapor Deposition Process,” Chemistry of Materials, **22**(9), pp. 2864–2868.

[17] Fabretto, M., Zuber, K., Hall, C., Murphy, P., and Griesser, H. J., 2009, “The Role of Water in the Synthesis and Performance of Vapour Phase Polymerised PEDOT Electrochromic Devices,” Journal of Materials Chemistry, **19**(42), pp. 7871–7878.

[18] Barr, M. C., Rowehl, J. A., Lunt, R. R., Xu, J., Wang, A., Boyce, C. M., Im, S. G., Bulović, V., and Gleason, K. K., 2011, “Direct Monolithic Integration of Organic Photovoltaic Circuits on Unmodified Paper,” Advanced Materials, **23**(31), pp. 3500–3505.

[19] Howden, R. M., Flores, E. J., Bulović, V., and Gleason, K. K., 2013, “The Application of Oxidative Chemical Vapor Deposited (OCVD) PEDOT to Textured and Non-Planar Photovoltaic Device Geometries for Enhanced Light Trapping,” Organic Electronics: physics, materials, applications, **14**(9), pp. 2257–2268.

[20] Ghaffari, M., Kosolwattana, S., Zhou, Y., Lachman, N., Lin, M., Bhattacharya, D., Gleason, K. K., Wardle, B. L., and Zhang, Q. M., 2013, “Hybrid Supercapacitor Materials from Poly(3,4-Ethylenedioxythiophene) Conformally Coated Aligned Carbon Nanotubes,” Electrochimica Acta, **112**, pp. 522–528.

[21] Im, S. G., Gleason, K. K., and Olivetti, E. A., 2007, “Doping Level and Work Function Control in Oxidative Chemical Vapor Deposited Poly (3,4-Ethylenedioxythiophene),” Applied Physics Letters, **90**(15), pp. 1–4.

[22] Goktas, H., Wang, X., Ugur, A., and Gleason, K. K., 2015, “Water-Assisted Vapor Deposition of PEDOT Thin Film,” Macromolecular Rapid Communications, **36**(13), pp. 1283–1289.

[23] Howden, R. M., McVay, E. D., and Gleason, K. K., 2013, “OCVD Poly(3,4-Ethylenedioxythiophene) Conductivity and Lifetime Enhancement via Acid Rinse Dopant Exchange,” Journal of Materials Chemistry A, **1**(4), pp. 1334–1340.

[24] Cahill, D. G., 1990, “Thermal Conductivity Measurement from 30 to 750 K: The 3ω Method,” Review of Scientific Instruments, **61**(2), pp. 802–808.

[25] Borca-Tasciuc, T., Kumar, A. R., and Chen, G., 2001, “Data Reduction in 3ω Method for Thin-Film Thermal Conductivity Determination,” Review of Scientific Instruments, **72**(4), pp. 2139–2147.

[26] Banerjee, K., Wu, G., Igeta, M., Amerasekera, A., Majumdar, A., and Hu, C., 1999, “Investigation of Self-Heating Phenomenon in Small Geometry Vias Using Scanning Joule Expansion Microscopy,” Annual Proceedings - Reliability Physics (Symposium), pp. 297–302.

[27] Poirier, D. R., and Geiger, G. H., 2016, “Conduction of Heat in Solids,” *Transport Phenomena in Materials Processing*, Springer International Publishing, Cham, pp. 281–327.

[28] Cahill, D. G., and Pohl, R. O., 1987, “Thermal Conductivity of Amorphous Solids above the Plateau,” Physical Review B, **35**(8), pp. 4067–4073.

[29] Cahill, D. G., Katiyar, M., and Abelson, J. R., 1994, “Thermal Conductivity of A-Si:H Thin Films,” Phys. Rev. B, **50**(9), pp. 6077–6081.

[30] Kaul, P. B., Day, K. A., and Abramson, A. R., 2007, “Application of the Three Omega Method for the Thermal Conductivity Measurement of Polyaniline,” Journal of Applied Physics, **101**(8).

[31] Kline, S. J., and McClintock, F. A., 1953, “Describing Uncertainties in Single-Sample Experiments,” Mechanical Engineering, **75**(1), pp. 3–8.

[32] Smith, P. M., Su, L., Gong, W., Nakamura, N., Reeja-Jayan, B., and Shen, S., 2018, “Thermal Conductivity of Poly(3,4-Ethylenedioxythiophene) Films Engineered by Oxidative Chemical Vapor Deposition (OCVD),” RSC Advances, **8**(35), pp. 19348–19352.

[33] Bhattacharyya, D., Howden, R. M., Borrelli, D. C., and Gleason, K. K., 2012, “Vapor Phase Oxidative Synthesis of Conjugated Polymers and Applications,” Journal of Polymer Science, Part B: Polymer Physics, **50**(19), pp. 1329–1351.

[34] Xu, B., Gopalan, S. A., Gopalan, A. I., Muthuchamy, N., Lee, K. P., Lee, J. S., Jiang, Y., Lee, S. W., Kim, S. W., Kim, J. S., Jeong, H. M., Kwon, J. B., Bae, J. H., and Kang, S. W., 2017, “Functional Solid Additive Modified PEDOT:PSS as an

Anode Buffer Layer for Enhanced Photovoltaic Performance and Stability in Polymer Solar Cells," Scientific Reports, **7**(October 2016), pp. 1–13.

[35] Zhou, S., Yang, Z., Gao, P., Li, X., Yang, X., Wang, D., He, J., Ying, Z., and Ye, J., 2016, "Wafer-Scale Integration of Inverted Nanopyramid Arrays for Advanced Light Trapping in Crystalline Silicon Thin Film Solar Cells," Nanoscale Research Letters, **11**(1), pp. 0–7.

[36] Baxamusa, S. H., and Gleason, K. K., 2008, "Thin Polymer Films with High Step Coverage in Microtrenches by Initiated CVD," Chemical Vapor Deposition, **14**(9–10), pp. 313–318.

[37] Goktas, H., Wang, X., Boscher, N. D., Torosian, S., and Gleason, K. K., 2016, "Functionalizable and Electrically Conductive Thin Films Formed by Oxidative Chemical Vapor Deposition (OCVD) from Mixtures of 3-Thiopheneethanol (3TE) and Ethylene Dioxythiophene (EDOT)," J. Mater. Chem. C, **4**(16), pp. 3403–3414.

[38] Im, S. G., and Gleason, K. K., 2007, "Systematic Control of the Electrical Conductivity of Poly(3,4- Ethylenedioxythiophene) via Oxidative Chemical Vapor Deposition," Macromolecules, **40**(18), pp. 6552–6556.

[39] Petruczok, C. D., Yang, R., and Gleason, K. K., 2013, "Controllable Cross-Linking of Vapor-Deposited Polymer Thin Films and Impact on Material Properties," Macromolecules, **46**(5), pp. 1832–1840.

[40] Reeves, G. K., and Harrison, H. B., 1982, "Obtaining the Specific Contact Resistance from Transmission Line Model Measurements," IEEE Electron Device Letters, **3**(5), pp. 111–113.

[41] Choy, C. L., 1977, "Thermal Conductivity of Polymers," Polymer, **18**(10), pp. 984–1004.

[42] Bubnova, O., Khan, Z. U., Malti, A., Braun, S., Fahlman, M., Berggren, M., and Crispin, X., 2011, "Optimization of the Thermoelectric Figure of Merit in the Conducting Polymer Poly(3,4-Ethylenedioxythiophene)," Nature Materials, **10**(6), pp. 429–433.

[43] Kim, G. H., Shao, L., Zhang, K., and Pipe, K. P., 2013, "Engineered Doping of Organic Semiconductors for Enhanced Thermoelectric Efficiency," Nature Materials, **12**(8), pp. 719–723.

[44] Zhang, T., and Luo, T., 2016, "Role of Chain Morphology and Stiffness in Thermal Conductivity of Amorphous Polymers," Journal of Physical Chemistry B, **120**(4), pp. 803–812.

[45] Chen, N., Reeja-Jayan, B., Lau, J., Moni, P., Liu, A., Dunn, B., and Gleason, K. K., 2015, "Nanoscale, Conformal Polysiloxane Thin Film Electrolytes for Three-Dimensional Battery Architectures," Materials Horizons, **2**(3), pp. 309–314.

[46] Eslamian, M., 2017, “Inorganic and Organic Solution-Processed Thin Film Devices,” Nano-Micro Letters, **9**(1), pp. 1–23.

[47] Sachan, S., Wankhede, S., and Kumar, V., 2020, “Organic Electronic Market by Material (Semiconductor, Conductive and Dielectric & Substrate), and Application (Display, Lighting, Battery, Conductive Ink and Others): Global Opportunity Analysis and Industry Forecast, 2020–2027,” Allied Market Research.

[48] Gevorgyan, S. A., and Krebs, F. C., 2008, “Bulk Heterojunctions Based on Native Polythiophene,” Chemistry of Materials, **20**(13), pp. 4386–4390.

[49] Zhang, T., Wu, X., and Luo, T., 2014, “Polymer Nanofibers with Outstanding Thermal Conductivity and Thermal Stability: Fundamental Linkage between Molecular Characteristics and Macroscopic Thermal Properties,” Journal of Physical Chemistry C, **118**(36), pp. 21148–21159.

[50] Nejati, S., and Lau, K. K. S., 2011, “Chemical Vapor Deposition Synthesis of Tunable Unsubstituted Polythiophene,” Langmuir, **27**(24), pp. 15223–15229.

[51] Lee, S., Borrelli, D. C., and Gleason, K. K., 2016, “Air-Stable Polythiophene-Based Thin Film Transistors Processed Using Oxidative Chemical Vapor Deposition: Carrier Transport and Channel/Metallization Contact Interface,” Organic Electronics: physics, materials, applications, **33**, pp. 253–262.

[52] Furukawa, Y., Akimoto, M., and Harada, I., 1987, “Vibrational Key Bands and Electrical Conductivity of Polythiophene,” Synthetic Metals, **18**(1–3), pp. 151–156.

[53] Mehrotra, P., 2016, “Biosensors and Their Applications - A Review,” Journal of Oral Biology and Craniofacial Research, **6**(2), pp. 153–159.

[54] Bhalla, N., Jolly, P., Formisano, N., and Estrela, P., 2016, “Introduction to Biosensors,” Essays in Biochemistry, **60**(1), pp. 1–8.

[55] Sakamoto, S., Putalun, W., Vimolmangkang, S., Phoolcharoen, W., Shoyama, Y., Tanaka, H., and Morimoto, S., 2018, “Enzyme-Linked Immunosorbent Assay for the Quantitative/Qualitative Analysis of Plant Secondary Metabolites,” Journal of natural medicines, **72**(1), pp. 32–42.

[56] Ahmed, F. E., Wiley, J. E., Weidner, D. A., Bonnerup, C., and Mota, H., 2010, “Surface Plasmon Resonance (SPR) Spectrometry as a Tool to Analyze Nucleic Acid-Protein Interactions in Crude Cellular Extracts,” Cancer Genomics and Proteomics, **7**(6), pp. 303–310.

[57] Xiao, Y., and Isaacs, S. N., 2012, “Enzyme-Linked Immunosorbent Assay (ELISA) and Blocking with Bovine Serum Albumin (BSA)—Not All BSAs Are Alike,” Journal of Immunological Methods, **384**(1–2), pp. 148–151.

[58] Masson, J. F., Battaglia, T. M., Cramer, J., Beaudoin, S., Sierks, M., and Booksh, K. S., 2006, “Reduction of Nonspecific Protein Binding on Surface

Plasmon Resonance Biosensors," Analytical and Bioanalytical Chemistry, **386**(7–8), pp. 1951–1959.

[59] Charles, P. T., Stubbs, V. R., Soto, C. M., Martin, B. D., White, B. J., and Taitt, C. R., 2009, "Reduction of Non-Specific Protein Adsorption Using Poly(Ethylene) Glycol (PEG) Modified Polyacrylate Hydrogels in Immunoassays for Staphylococcal Enterotoxin B Detection," Sensors, **9**(1), pp. 645–655.

[60] Kenna, J. G., Major, G. N., and Williams, R. S., 1985, "Methods for Reducing Non-Specific Antibody Binding in Enzyme-Linked Immunosorbent Assays," Journal of Immunological Methods, **85**(2), pp. 409–419.

[61] Lange, U., and Mirsky, V. M., 2011, "Chemiresistors Based on Conducting Polymers: A Review on Measurement Techniques," Analytica Chimica Acta, **687**(2), pp. 105–113.

[62] Hai, W., Goda, T., Takeuchi, H., Yamaoka, S., Horiguchi, Y., Matsumoto, A., and Miyahara, Y., 2017, "Specific Recognition of Human Influenza Virus with PEDOT Bearing Sialic Acid-Terminated Trisaccharides," ACS Applied Materials and Interfaces, **9**(16), pp. 14162–14170.

[63] Bhattacharyya, D., Senecal, K., Marek, P., Senecal, A., and Gleason, K. K., 2011, "High Surface Area Flexible Chemiresistive Biosensor by Oxidative Chemical Vapor Deposition," Advanced Functional Materials, **21**(22), pp. 4328–4337.

[64] Winther-Jensen, B., Chen, J., West, K., and Wallace, G., 2004, "Vapor Phase Polymerization of Pyrrole and Thiophene Using Iron(III) Sulfonates as Oxidizing Agents," Macromolecules, **37**(16), pp. 5930–5935.

[65] Skorenko, K. H., Faucett, A. C., Liu, J., Ravvin, N. A., Bernier, W. E., Mativetsky, J. M., and Jones, W. E., 2015, "Vapor Phase Polymerization and Mechanical Testing of Highly Electrically Conductive Poly(3,4-Ethylenedioxythiophene) for Flexible Devices," Synthetic Metals, **209**, pp. 297–303.

[66] Jones, W. E., Madl, C. M., Kariuki, P. N., Gendron, J., and Piper, L. F. J., 2011, "Vapor Phase Polymerization of Poly (3,4-Ethylenedioxythiophene) on Flexible Substrates for Enhanced Transparent Electrodes," Synthetic Metals, **161**(13–14), pp. 1159–1165.

[67] Piran, U., and Riordan, W. J., 1990, "Dissociation Rate Constant of the Biotin-Streptavidin Complex," Journal of Immunological Methods, **133**(1), pp. 141–143.

[68] GREEN, N., 1963, "AVIDIN. 1. THE USE OF [14C]BIOTIN FOR KINETIC STUDIES AND FOR ASSAY," Biochemical Journal, **89**(3), pp. 585–591.

[69] Gallo, D., Diggs, J. L., Shell, G. R., Dailey, P. J., Hoffman, M. N., and Riggs, J. L., 1986, “Comparison of Detection of Antibody to the Acquired Immune Deficiency Syndrome Virus by Enzyme Immunoassay, Immunofluorescence, and Western Blot Methods,” Journal of Clinical Microbiology, **23**(6), pp. 1049–1051.

[70] Jeon, M., Kim, J., Paeng, K. J., Park, S. W., and Paeng, I. R., 2008, “Biotin-Avidin Mediated Competitive Enzyme-Linked Immunosorbent Assay to Detect Residues of Tetracyclines in Milk,” Microchemical Journal, **88**(1), pp. 26–31.

[71] Hochegger, R., Mayer, W., and Prochaska, M., 2015, “Comparison of R5 and G12 Antibody-Based ELISA Used for the Determination of the Gluten Content in Official Food Samples,” Foods, **4**(4), pp. 654–664.

[72] Im, S. G., Yoo, P. J., Hammond, P. T., and Gleason, K. K., 2007, “Grafted Conducting Polymer Films for Nano-Patterning onto Various Organic and Inorganic Substrates by Oxidative Chemical Vapor Deposition,” Advanced Materials, **19**(19), pp. 2863–2867.

[73] Wang, X., Hou, S., Goktas, H., Kovacik, P., Yaul, F., Paidimarri, A., Ickes, N., Chandrakasan, A., and Gleason, K., 2015, “Small-Area, Resistive Volatile Organic Compound (VOC) Sensors Using Metal-Polymer Hybrid Film Based on Oxidative Chemical Vapor Deposition (OCVD),” ACS Applied Materials and Interfaces, **7**(30), pp. 16213–16222.

[74] Vaddiraju, S., and Gleason, K. K., 2010, “Selective Sensing of Volatile Organic Compounds Using Novel Conducting Polymer-Metal Nanoparticle Hybrids,” Nanotechnology, **21**(12).

[75] Su, L., Smith, P. M., Anand, P., and Reeja-Jayan, B., 2018, “Surface Engineering of a LiMn2O4 Electrode Using Nanoscale Polymer Thin Films via Chemical Vapor Deposition Polymerization,” ACS Applied Materials and Interfaces, **10**(32), pp. 27063–27073.

[76] Shi, J. L., Qi, R., Zhang, X. D., Wang, P. F., Fu, W. G., Yin, Y. X., Xu, J., Wan, L. J., and Guo, Y. G., 2017, “High-Thermal- and Air-Stability Cathode Material with Concentration-Gradient Buffer for Li-Ion Batteries,” ACS Applied Materials and Interfaces, **9**(49), pp. 42829–42835.

[77] Liu, J., Reeja-Jayan, B., and Manthiram, A., 2010, “ Conductive Surface Modification with Aluminum of High Capacity Layered Li[Li 0.2 Mn 0.54 Ni 0.13 Co 0.13]O 2 Cathodes ,” The Journal of Physical Chemistry C, **114**(20), pp. 9528–9533.

[78] Beaulieu, J. M., and Gainetdinov, R. R., 2011, “The Physiology, Signaling, and Pharmacology of Dopamine Receptors,” Pharmacological Reviews, **63**(1), pp. 182–217.

[79] Volkow, N. D., Fowler, J. S., Wang, G. J., Swanson, J. M., and Telang, F., 2007, “Dopamine in Drug Abuse and Addiction: Results of Imaging Studies and Treatment Implications,” Archives of Neurology, **64**(11), pp. 1575–1579.

[80] Zhang, X., Chen, X., Kai, S., Wang, H.-Y., Yang, J., Wu, F.-G., and Chen, Z., 2015, “Highly Sensitive and Selective Detection of Dopamine Using One-Pot Synthesized Highly Photoluminescent Silicon Nanoparticles,” Analytical Chemistry, **87**(6), pp. 3360–3365.

[81] Jackowska, K., and Krysinski, P., 2013, “New Trends in the Electrochemical Sensing of Dopamine,” Analytical and Bioanalytical Chemistry, **405**(11), pp. 3753–3771.

[82] Liu, D., Rahman, Md. M., Ge, C., Kim, J., and Lee, J.-J., 2017, “Highly Stable and Conductive PEDOT:PSS/Graphene Nanocomposites for Biosensor Applications in Aqueous Medium,” New Journal of Chemistry, **41**(24), pp. 15458–15465.

[83] Shang, N. G., Papakonstantinou, P., McMullan, M., Chu, M., Stamboulis, A., Potenza, A., Dhesi, S. S., and Marchetto, H., 2008, “Catalyst-Free Efficient Growth, Orientation and Biosensing Properties of Multilayer Graphene Nanoflake Films with Sharp Edge Planes,” Advanced Functional Materials, **18**(21), pp. 3506–3514.

[84] Chen, C.-H., and Luo, S.-C., 2015, “Tuning Surface Charge and Morphology for the Efficient Detection of Dopamine under the Interferences of Uric Acid, Ascorbic Acid, and Protein Adsorption,” ACS Applied Materials & Interfaces, **7**(39), pp. 21931–21938.

[85] Garg, R., Rastogi, S. K., Lamparski, M., de la Barrera, S. C., Pace, G. T., Nuhfer, N. T., Hunt, B. M., Meunier, V., and Cohen-Karni, T., 2017, “Nanowire-Mesh-Templated Growth of Out-of-Plane Three-Dimensional Fuzzy Graphene,” ACS Nano, **11**(6), pp. 6301–6311.

[86] Chen, G., Xu, Y., Song, B., Wang, X., Zhou, J., Gleason, K. K., Lee, E. M. Y., Huberman, S., and Jiang, Z., 2018, “Molecular Engineered Conjugated Polymer with High Thermal Conductivity,” Science Advances, **4**(3), p. eaar3031.

[87] Perepichka, I. F., and Perepichka, D. F., 2009, *Handbook of Thiophene-Based Materials*, John Wiley & Sons, Ltd, Chichester, UK.

[88] Bhattacharyya, D., Yang, R., and Gleason, K. K., 2012, “High Aspect Ratio, Functionalizable Conducting Copolymer Nanobundles,” Journal of Materials Chemistry, **22**(33), pp. 17147–17152.

[89] Bhattacharyya, D., and Gleason, K. K., 2011, “Single-Step Oxidative Chemical Vapor Deposition of COOH Functional Conducting Copolymer and Immobilization

of Biomolecule for Sensor Application," Chemistry of Materials, **23**(10), pp. 2600–2605.

[90] Borrelli, D. C., Barr, M. C., Bulović, V., and Gleason, K. K., 2012, "Bilayer Heterojunction Polymer Solar Cells Using Unsubstituted Polythiophene via Oxidative Chemical Vapor Deposition," Solar Energy Materials and Solar Cells, **99**, pp. 190–196.

[91] Mirabedin, M., Vergnes, H., Caussé, N., Vahlas, C., and Caussat, B., 2020, "An out of the Box Vision over Oxidative Chemical Vapor Deposition of PEDOT Involving Sublimed Iron Trichloride," Synthetic Metals, **266**(April), p. 116419.

[92] Smolin, Y. Y., van Aken, K. L., Boota, M., Soroush, M., Gogotsi, Y., and Lau, K. K. S., 2017, "Engineering Ultrathin Polyaniline in Micro/Mesoporous Carbon Supercapacitor Electrodes Using Oxidative Chemical Vapor Deposition," Advanced Materials Interfaces, **4**(8).

[93] Nejati, S., Minford, T. E., Smolin, Y. Y., and Lau, K. K. S., 2014, "Enhanced Charge Storage of Ultrathin Polythiophene Films within Porous Nanostructures," ACS Nano, **8**(6), pp. 5413–5422.

[94] Li, X., Rafie, A., Smolin, Y. Y., Simotwo, S., Kalra, V., and Lau, K. K. S., 2019, "Engineering Conformal Nanoporous Polyaniline via Oxidative Chemical Vapor Deposition and Its Potential Application in Supercapacitors," Chemical Engineering Science, **194**, pp. 156–164.

[95] Kaviani, S., Mohammadi Ghaleni, M., Tavakoli, E., and Nejati, S., 2019, "Electroactive and Conformal Coatings of Oxidative Chemical Vapor Deposition Polymers for Oxygen Electroreduction," ACS Applied Polymer Materials, **1**(3), pp. 552–560.

[96] Nejati, S., and Lau, K. K. S., 2011, "Chemical Vapor Deposition Synthesis of Tunable Unsubstituted Polythiophene," Langmuir, **27**(24), pp. 15223–15229.